

Revisiting Robust Model Fitting Using Truncated Loss

Fei Wen, Hewen Wei, Yipeng Liu, and Peilin Liu

Abstract—Robust fitting is a fundamental problem in low-level vision, which is typically achieved by maximum consensus (MC) estimators to identify inliers first or by M-estimators directly. While these two methods are discriminately preferred in different applications, truncated loss based M-estimators are similar to MC as they can also identify inliers. This work revisits a formulation that achieves simultaneous inlier identification and model estimation (SIME) using truncated loss. It has a generalized form adapts to both linear and nonlinear residual models. We show that as SIME takes fitting residual into account in finding inliers, its lowest achievable residual in model fitting is lower than that of MC robust fitting. Then, an alternating minimization (AM) algorithm is employed to solve the SIME formulation. Meanwhile, a semidefinite relaxation (SDR) embedded AM algorithm is developed in order to ease the high nonconvexity of the SIME formulation. Furthermore, the new algorithms are applied to various 2D/3D registration problems. Experimental results show that the new algorithms significantly outperform RANSAC and deterministic approximate MC methods at high outlier ratios. Besides, in rotation and Euclidean registration problems, the new algorithms also compare favorably with state-of-the-art registration methods, especially in high noise and outliers. Code is available at <https://github.com/FWen/mcme.git>.

Index Terms—Maximum consensus, robust fitting, homography estimation, rotation registration, point-cloud registration, outlier removal.

1 Introduction

Robust fitting is a fundamental problem in low-level vision to process raw data in the presence of outliers, which plays a critical role in modern vision geometry [1]–[4]. For robust fitting, the maximum consensus (MC) criterion and the M-estimation are of the most popular and widely used. Given a set of raw measurements, MC aims to find a model that has the largest consensus on the measurements. In comparison, M-estimation resorts to robust loss functions that insensitive to outliers to estimate the model directly.

There exist a number of MC methods, including randomized methods, global methods and deterministic approximate methods. Randomized methods, such as the classic RANSAC method [5] and its many variants [6]–[10], [57], [58], typically use a hypothesize-and-verify procedure to fit the model on randomly sampled subsets and verify the model based on the size of measurements consistent with the model. A significant feature of randomized methods is that their solution quality is guaranteed in probability depending on iteration number. In practical applications with affordable finite iterations, the solution quality is unpredictable and can be random in different runs due to their randomized nature. Global methods aim to find an optimum solution by global optimization algorithms.

As the MC problem is intrinsically a combinatorial optimization problem, global optimum can only be guaranteed by searching based algorithms, such as branch-and-bound (BnB) search [11]–[13], tree search [14], and enumeration [15], [16]. Though optimum solution can be achieved, global methods do not scale to moderate to high dimensional problems. Deterministic approximate methods solve the MC problem approximately and deterministically, such as the convex relaxed method [17], reweighted ℓ_1 method [18], ℓ_0 method [19], and exact penalty (EP) method [20], [21]. Moreover, deterministic outlier removal methods using ℓ_∞ norm have been proposed in [22], [23]. These methods are computationally much more efficient than global methods, and meanwhile, some of them can achieve better solution quality than randomized methods [21].

M-estimation is another well-known framework for robust fitting [26]–[30]. While MC robust fitting typically has two steps, firstly finding a consensus set of inliers and then fitting a model on the consensus set, M-estimators directly estimate a model using a robust loss function (e.g., the Huber norm). Generally, MC and M-estimators are discriminately preferred in different applications. In some applications M-estimators can be efficiently solved by the iteratively reweighted least-squares (IRLS) algorithm. However, there also exist some applications the weighted least-squares (LS) problem is not efficiently solvable, e.g., projective transformation estimation with geometric distances.

Among M-estimators, truncated loss based ones have two distinct features, high break-down point and applicable to inliers/outliers identification. M-estimation using truncated LS loss can be traced back to the works [59]–[61]. Recently, it has been used to develop various methods for 2D/3D registration [29], [31], [41], [51]. In [41], a piecewise constant approximation of truncated LS loss has

- F. Wen and P. Liu are with the Department of Electronic Engineering, Shanghai Jiao Tong University, Shanghai, China, 200240. E-mail: wenfei@sjtu.edu.cn; liupeilin@sjtu.edu.cn.
- H. Wei is with Shanghai branch of the Southwest Institute of Electronics and Telecommunication Technology of China, Shanghai, China, 200434. Email: weihewen@tsinghua.org.cn. Y. Liu is with the School of Electronic Engineering, University of Electronic Science and Technology of China, Chengdu, China, 611731. E-mail: yipengliu@uestc.edu.cn.

Manuscript received xx, xx, 2020.

been used and an exhaustive search algorithm has been proposed. In [31], semi-definite relaxation (SDR) has been used to solve truncated LS loss based Wahba problem, which can tolerate extreme amounts of outliers. However, the algorithm does not scale well with problem size. Then, an efficient algorithm has been proposed in [29] based on graduated non-convexity (GNC) scheme, with some compromise on the tolerance against outliers. More recently, a fast and certifiable algorithm has been developed for point cloud registration in [51]. It decouples the scale, rotation and translation estimation, and solves them separately and sequentially to achieve high effectiveness and efficiency.

This work investigates an M-estimation formulation that uses truncated loss to achieve simultaneous inlier identification and model estimation (SIME). Characteristically, while most M-estimators do not apply to the MC problem, SIME can identify inliers/outliers based on whether the fitting residual exceeding the truncating threshold, which is similar to the MC criterion. The main contributions of this work are as follows.

First, we investigate a generalized truncated loss based SIME formulation, which adapts to both linear and nonlinear residual models in various vision problems. Particularly, we theoretically show that the lowest achievable fitting residual of SIME is lower than that of MC robust fitting. It is due the fact that SIME takes the distribution of fitting residual into account in identifying inliers, while MC does not. Second, we propose two algorithms for the SIME formulation, one is based on the direct alternating minimization (AM) algorithm, and the other additionally uses an SDR of the binary variables in an attempt to ease the high non-convexity of the problem. For the latter, the sparsity of the problem is exploited in combination with low-rank factorization to achieve high efficiency. Third, we apply the new algorithms to various problems, including robust linear regression, projective transformation estimation with algebraic and geometric distances (e.g., homography and affinity estimation), rotation registration, and 6-DoF Euclidean registration. Finally, experimental results on various 2D and 3D registration problems are provided to demonstrate the favorable performance of SIME in comparison with previous state-of-the-art.

Notations: $\mathbb{I}(\cdot) \in \{0, 1\}$ is the indicator function. \otimes and \circ stand for the Kronecker product and quaternion product, respectively. $\mathbf{1}_N$ is an N dimension vector with all elements being unit, and $\mathbf{0}$ is a zero vector or matrix with a proper size. $\|\cdot\|$ and $\|\cdot\|_p$ denotes the Euclidean and ℓ_p norm, respectively. $(\cdot)^T$ denotes transpose. \mathbb{S}^N is the set of $N \times N$ real-valued symmetric matrices. For $\mathbf{X} \in \mathbb{S}^N$, $\mathbf{X} \succeq \mathbf{0}$ means that \mathbf{X} is semidefinite. Both $\mathbf{X}(i, j)$ and $X_{i,j}$ denote the (i, j) -th element of the matrix \mathbf{X} . $\text{vec}(\cdot)$ is the vectorization operation of a matrix.

2 Proposed Formulation

2.1 SIME Using Truncated Loss

Truncated loss based M-estimation can be traced back to the works [59]–[61], where truncated LS loss is used to construct robust estimators with influence functions going to zero. Recently, truncated LS loss has been used to develop robust algorithms for rotation searching [31] and point cloud

registration [51], which can tolerate extreme amounts of outliers.

Given a set of N measurements, let Φ denote a generalized loss function to be truncated and β denote the truncating level. Using such a truncated loss to estimate a mode parameterized by $\theta \in \mathbb{R}^d$, the formulation considered in this work is

$$\begin{aligned} \text{SIME : } \min_{\theta \in \mathbb{R}^d, s \in \{0, 1\}^N} & \sum_{i=1}^N (1-s_i)\Phi(r_i(\theta)) + \beta s_i \\ \text{s.t. } & h(\theta) = 0, \end{aligned} \quad (1)$$

where $r_i(\theta)$ gives the non-negative residual of the i -th measurement with respect to θ . $h(\theta) = 0$ is a constraint on the model parameter. For example, as will be detailed in Section 4, a constraint $\|\theta\| = 1$ is present in rotation registration and Euclidean registration problems, in which case $h(\theta) = \|\theta\| - 1$. The objective in (1) is a truncated cost as $\min_{s_i \in \{0, 1\}} (1-s_i)\Phi(\cdot) + \beta s_i$ is equivalent to $\min(\Phi(\cdot), \beta)$ [31]. When Φ is the LS loss, problem (1) without the constraint $h(\theta) = 0$ becomes the minimum truncated LS formulation [60].

Note that we consider a generalized truncated loss rather than the truncated LS loss. The reason is twofold. First, as will be detailed in Section 3 and 4, a generalized Φ makes SIME applicable to nonlinear geometric residual model arising in multi-view geometry problems. Though nonlinear, such residual model is geometrically and statistically meaningful, hence is widely used in multi-view geometry problems [37]. Second, while the LS loss is optimal for Gaussian noise, a generalized Φ also adapts to ℓ_p loss with $p < 2$, which is desirable when the inlier noise is not Gaussian but super-Gaussian (detailed in Appendix C).

A feature of SIME is it can identify inliers/outliers based on the solution s , which is similar to the MC criterion. Given a set of N measurements, MC aims to find a feasible model parameterized by θ , that is consistent with as many of the measurements as possible up to an inlier residual threshold $\tau > 0$, i.e., has the largest consensus set I as [1]

$$\begin{aligned} \text{MC : } \max_{\theta \in \mathbb{R}^d, I \subseteq \Omega} & |I| \\ \text{s.t. } & r_i(\theta) \leq \tau, \quad \forall i \in I, \quad h(\theta) = 0, \end{aligned} \quad (2)$$

where $\Omega = \{1, 2, \dots, N\}$ is the index set of the measurements. Let I^* be a solution of (2), then I^* stands for the index set of the true inliers, while the complementary set of I^* , denoted by $\Omega \setminus I^*$, stands for the index set of the true outliers. Using some auxiliary binary variables $s = [s_1, \dots, s_N]^T \in \{0, 1\}^N$, (2) can be reformulated into

$$\begin{aligned} \min_{\theta \in \mathbb{R}^d, s \in \{0, 1\}^N} & \sum_{i=1}^N s_i \\ \text{s.t. } & r_i(\theta) \leq \tau + s_i L, \quad \forall i \in \Omega, \quad h(\theta) = 0, \end{aligned} \quad (3)$$

where L is a sufficiently large positive constant.

The similarity and difference between SIME and MC can be observed from (1) and (3). Similar to SIME, for a solution of MC, the i -th measurement is identified as an outlier if $s_i = 1$, or an inlier if $s_i = 0$. While MC does not take the inlier residual into account in inlier identification, SIME takes that into consideration via simultaneous inlier identification and model fitting in a single step. Besides, unlike that the θ solution of MC is only a feasible solution

satisfying the residual constraint, the θ solution of SIME is the desired model fitting result on the identified inliers.

SIME uses β to balance the number of outliers against the fitting residual, by which the residual constraint in MC is removed. Obviously, a larger β would result in a larger number of s_i 's being zero, i.e., more identified inliers (which are not necessary to be true inliers). That is a too large β would yield a larger consensus size than I^* and include some true outliers, while a too small β would yield a smaller consensus size than I^* and exclude some true inliers. As SIME estimates the model only using the measurements with residuals less than β , β can be easily selected as a threshold which tightly upper bounds the fitting residual of the true inliers. For example, if there exists a proper bound τ such that $r_i(\theta) \leq \tau$ for $\forall i \in I^*$ with a high probability for the true model, it is reasonable to choose $\beta = \Phi(\tau)$.

The following result shows SIME can be viewed as an approximate maximum likelihood (ML) estimator under certain distribution assumption of inliers and outliers.

Proposition 1. Denote $r_i = r_i(\theta)$ for succinctness. SIME is an approximate ML estimator under conditions:

- i) For any true inliers, i.e. $\forall i \in I^*$, r_i follows a zero-mean exponential distribution (from the natural exponential family) as $r_i \sim \mathcal{N}(0, \sigma_i) = \exp(-\Phi(r_i, \sigma_i))$ for some scale parameter $\sigma_i > 0$, where Φ is an increasing function of r_i on $[0, +\infty)$. The model θ is constrained as $h(\theta) = 0$.
- ii) For any true outliers, i.e. $\forall i \in \Omega \setminus I^*$, r_i follows a uniform distribution on the interval $[\tau, u]$, where u is the possible maximal perturbation of outliers.

Proof: Let $P \in (0, 1]$ and $(1 - P) \in [0, 1)$ denote the probability of inliers and outliers, respectively. Under conditions i) and ii), the likelihood of $\mathbf{r} = [r_1, r_2, \dots, r_N]^T$ is given by

$$\mathcal{L}(\mathbf{r}; \theta) = \prod_{i=1}^N [P \exp(-\Phi(r_i, \sigma_i))]^{1 - \mathbb{I}(\tau < r_i \leq u)} \times \left[P \exp(-\Phi(r_i, \sigma_i)) + \frac{1 - P}{u - \tau} \right]^{\mathbb{I}(\tau < r_i \leq u)},$$

with $h(\theta) = 0$. The corresponding log-likelihood is

$$\begin{aligned} \log \mathcal{L}(\mathbf{r}; \theta) &= \sum_{i=1}^N (1 - \mathbb{I}(\tau < r_i \leq u)) [-\Phi(r_i, \sigma_i) + \log P] \\ &\quad + \mathbb{I}(\tau < r_i \leq u) \underbrace{\log \left[P \exp(-\Phi(r_i, \sigma_i)) + \frac{1 - P}{u - \tau} \right]}_{L_o(r_i)}, \end{aligned} \quad (4)$$

with $h(\theta) = 0$. Since Φ is an increasing function, for $r_i \in (\tau, u]$ it follows that

$$\log(1 - P) - \log(u - \tau) < L_o(r_i) < L_o(\tau).$$

That is as r_i increases on $(\tau, u]$, $L_o(r_i)$ decreases from $L_o(\tau)$ toward $\log(1 - P) - \log(u - \tau)$. Meanwhile, for sufficiently large u , we have $\exp(-\Phi(r_i, \sigma_i)) \rightarrow 0$ for $r_i > u$. Hence, the likelihood is dominated by the two cases of $r_i \leq \tau$ and $\tau < r_i \leq u$, i.e., $r_i \leq u$. Then, from the fact that $\mathbb{I}(\tau < r_i \leq u)$ is equivalent to $\mathbb{I}(\Phi(\tau) < \Phi(r_i) \leq \Phi(u))$, it is easy to see that with some β satisfying $\log(1 - P) - \log(u - \tau) \leq \beta \leq L_o(\tau)$,

the minimization problem

$$\min_{\theta \in \mathbb{R}^d, s_i \in \{0, 1\}} \sum_{i=1}^N (1 - s_i) \Phi(r_i, \sigma_i) + \beta s_i,$$

can be viewed as an approximation of maximizing the log-likelihood (4). Under i.i.d assumption of inliers with $\sigma_i = \sigma$ for $\forall i \in I^*$, taking the scale parameter σ into β , and ignoring constant terms independent on r_i , it leads to (1).

Remark 1. This proposition indicates that SIME is an approximate ML estimator under the conditions that, the inlier noise is relatively small and follows a natural exponential distribution, while the outliers contain large perturbation following a uniform distribution. The natural exponential family includes a large class of distributions, e.g., for zero-mean Gaussian distribution $\Phi(r_i, \sigma_i) = \frac{r_i^2}{2\sigma_i^2} + \frac{1}{2} \log(2\pi\sigma_i^2)$. Besides, it also adapts to super-Gaussian distribution, for which $\Phi(r_i) \propto r_i^p$ with $p < 2$, meaning that the ℓ_p loss should be used when the inlier noise is super-Gaussian.

2.2 Comparison between MC and SIME

This subsection compares MC with SIME to show that they can produce the same inlier set in special conditions, but not in general conditions. Particularly, SIME has lower fitting residual than MC fitting.

Before proceeding to the results, we present some definitions will be used in the analysis. Denote

$$\theta_I := \arg \min_{\theta \in \mathbb{R}^d, h(\theta)=0} \sum_{i \in I} \Phi(r_i(\theta)),$$

$$R(I) := \sum_{i \in I} \Phi(r_i(\theta_I)) = \min_{\theta \in \mathbb{R}^d, h(\theta)=0} \sum_{i \in I} \Phi(r_i(\theta)),$$

and the objective of SIME as

$$f(\theta, \mathbf{s}) := \sum_{i=1}^N (1 - s_i) \Phi(r_i(\theta)) + \Phi(\tau) s_i.$$

From the truncating property of the loss in (1), a solution of SIME with identified inlier set I must satisfies $\Phi(r_i(\theta_I)) \leq \Phi(\tau)$ for $\forall i \in I$ and $\Phi(r_i(\theta_I)) > \Phi(\tau)$ for $\forall i \in \Omega \setminus I$. Accordingly, we define a set of all possible inlier sets associated with feasible solutions of SIME as

$$F := \{I : \Phi(r_i(\theta_I)) \leq \Phi(\tau), \forall i \in I; \Phi(r_i(\theta_I)) > \Phi(\tau), \forall i \in \Omega \setminus I; I \subseteq \Omega\}.$$

For any $I \subseteq \Omega$, (θ_I, \mathbf{s}_I) is a feasible solution of SIME only when $I \in F$, where \mathbf{s}_I is a binary vector associated with I as

$$\mathbf{s}_I := [\mathbb{I}(1 \notin I), \mathbb{I}(2 \notin I), \dots, \mathbb{I}(N \notin I)]^T.$$

The following result gives a sufficient condition under which the two criterions produce the same consensus set.

Proposition 2. Suppose that $\beta = \Phi(\tau)$, and Φ is increasing on $[0, +\infty)$ with $\Phi(0) = 0$. Let I^* denote a solution of MC, and I^+ denote the inlier set of a SIME solution, then, I^+ is a consensus set and $|I^+| \leq |I^*|$. Particularly, if $\Phi(r_i(\theta_{I^*})) \leq \Phi(\tau)$, $\forall i \in I^*$, and for any other consensus set $I^\bullet \in F$ there holds

$$|I^*| - |I^\bullet| > (R(I^*) - R(I^\bullet))/\Phi(\tau), \quad (5)$$

then $I^+ = I^*$.

Proof: First, with $\beta = \Phi(\tau)$, it follows from (1) that any inlier set I^+ produced by SIME satisfies $\Phi(r_i(\theta_{I^+})) \leq \Phi(\tau)$

for $\forall i \in I^+$. As Φ is increasing on $[0, +\infty)$, $\Phi(r_i(\theta_{I^+})) \leq \Phi(\tau)$ is equivalent to $r_i(\theta_{I^+}) \leq \tau$. Thus, I^+ must be a consensus set satisfies $r_i(\theta) \leq \tau, \forall i \in I^+$ for some θ . Furthermore, since I^* is the maximum consensus set, the size of I^+ is upper bounded by the size of I^* , i.e. $|I^+| \leq |I^*|$. Under condition $\Phi(r_i(\theta_{I^*})) \leq \Phi(\tau), \forall i \in I^*$, since I^* is a maximum consensus set, it follows that $r_i(\theta_{I^*}) > \tau$ and hence $\Phi(r_i(\theta_{I^*})) > \Phi(\tau)$ for $\forall i \in \Omega \setminus I^*$, otherwise there exists another consensus set I' such that $I^* \subset I'$ and $|I^*| < |I'|$. Thus, $I^* \in F$ and $f(\theta_{I^*}, s_{I^*}) = R(I^*) + |\Omega \setminus I^*| \Phi(\tau)$. Moreover, for a consensus set I^\bullet satisfying $I^\bullet \in F$, which is a necessary condition for I^\bullet to be the inlier set of a feasible SIME solution, $f(\theta_{I^\bullet}, s_{I^\bullet}) = R(I^\bullet) + |\Omega \setminus I^\bullet| \Phi(\tau)$. Then, for any such consensus set $I^\bullet \neq I^*$ if it holds $f(\theta_{I^\bullet}, s_{I^\bullet}) > f(\theta_{I^*}, s_{I^*})$, (θ_{I^*}, s_{I^*}) is a solution of SIME which attains the minimum objective value, and the corresponding inlier set is given by I^* . This inequality condition holds if $R(I^\bullet) - |I^\bullet| \Phi(\tau) > R(I^*) - |I^*| \Phi(\tau)$, which is equivalent to the condition (5).

Remark 2. Another special condition for $I^+ = I^*$ in the case of truncated LS loss is given in [51, Lemma 23]. As I^* is the largest consensus set, it follows that $|I^*| \geq |I^\bullet|$ for any other consensus set I^\bullet . Then, it is easy to see that, with selection $\beta = \Phi(\tau)$, a condition for SIME to yield the same inlier set as MC is that the residual over I^* is very small (or relatively small compared with the residual over any I^\bullet) and the condition $\Phi(r_i(\theta_{I^*})) \leq \Phi(\tau)$ for $\forall i \in I^*$ is satisfied. However, they do not produce the same consensus set in general condition. Moreover, a sufficient (but not necessary) condition for $I^+ \neq I^*$ is $\Phi(r_i(\theta_{I^*})) > \Phi(\tau)$ for some $i \in I^*$, since in this case I^* is not a feasible solution of SIME, i.e. $I^* \notin F$.

As SIME takes the inlier residual distribution of model fitting into account, while MC does not, a natural question arises: What is the performance difference between SIME and MC? Next we answer this question by comparing the lowest achievable residual of the two criterions.

Theorem 3. Let I^+ denote the inlier set of a SIME solution and I^* denote a solution of MC. Suppose that Φ is monotone increasing on $[0, +\infty)$ with $\Phi(0) = 0$. Then, with $\beta = \Phi(\tau)$, the lowest achievable residual of SIME is lower than that of MC as

$$\min_{\theta \in \mathbb{R}^d, h(\theta)=0} \sum_{i \in I^+} \Phi(r_i(\theta)) \leq \min_{\theta \in \mathbb{R}^d, h(\theta)=0} \sum_{i \in I^*} \Phi(r_i(\theta)). \quad (6)$$

Furthermore, if $I^* \notin F$, the inequality in (6) holds strictly.

Proof: We consider two cases of the maximum consensus set I^* and prove Theorem 3 by contradiction.

Case 1: $\Phi(r_i(\theta_{I^*})) \leq \Phi(\tau), \forall i \in I^*$. Similar to the argumentation in proving Proposition 2, in this case $I^* \in F$ and (θ_{I^*}, s_{I^*}) is a feasible solution of SIME with objective value $f(\theta_{I^*}, s_{I^*}) = R(I^*) + |\Omega \setminus I^*| \Phi(\tau)$. Meanwhile, from Proposition 3, we have $|I^+| \leq |I^*|$ and hence $|\Omega \setminus I^+| \geq |\Omega \setminus I^*|$. As I^+ is the inlier set of a SIME solution, hence $I^+ \in F$. Then, if (6) does not hold, which implies $R(I^+) > R(I^*)$ and further

$$\begin{aligned} f(\theta_{I^+}, s_{I^+}) &= R(I^+) + |\Omega \setminus I^+| \Phi(\tau) \\ &> R(I^*) + |\Omega \setminus I^*| \Phi(\tau) = f(\theta_{I^*}, s_{I^*}). \end{aligned}$$

This inequality means that if (6) does not hold, the feasible solution (θ_{I^*}, s_{I^*}) attains a lower objective value of SIME

than (θ_{I^+}, s_{I^+}) . Obviously, it contradicts to that I^+ is the inlier set of a SIME solution, under which (θ_{I^+}, s_{I^+}) should attain the minimum objective value of SIME.

Case 2: For some $\hat{I}^* \subset I^*$, $\Phi(r_i(\theta_{\hat{I}^*})) \leq \Phi(\tau), \forall i \in \hat{I}^*$ and $\Phi(r_i(\theta_{I^*})) > \Phi(\tau), \forall i \in I^* \setminus \hat{I}^*$. In this case, though I^* is a consensus set, it no longer holds that $\Phi(r_i(\theta_{I^*})) > \Phi(\tau)$ for $\forall i \in \Omega \setminus I^*$, and (θ_{I^*}, s_{I^*}) is no longer a feasible solution of SIME, i.e. $I^* \notin F$, there must exist another consensus set $I' \in F$ such that $(\theta_{I'}, s_{I'})$ attains a lower objective value of SIME than (θ_{I^*}, s_{I^*}) as $R(I^*) + |\Omega \setminus I^*| \Phi(\tau) > R(I') + |\Omega \setminus I'| \Phi(\tau)$. If (6) does not hold strictly, i.e. $R(I^+) \geq R(I^*)$, then, with $|I^+| \leq |I^*|$, it follows that

$$\begin{aligned} f(\theta_{I^+}, s_{I^+}) &= R(I^+) + |\Omega \setminus I^+| \Phi(\tau) \\ &\geq R(I^*) + |\Omega \setminus I^*| \Phi(\tau) \\ &> R(I') + |\Omega \setminus I'| \Phi(\tau) = f(\theta_{I'}, s_{I'}), \end{aligned}$$

which implies that there exists another feasible solution $(\theta_{I'}, s_{I'})$ that can attain a lower objective value of SIME than (θ_{I^+}, s_{I^+}) . Obviously, it contradicts to that I^+ is the inlier set of a SIME solution with (θ_{I^+}, s_{I^+}) attaining the minimum objective value of SIME. Thus, when $I^* \notin F$, the inequality in (6) holds strictly.

Remark 3. This theorem sheds some light on the difference between SIME and MC in terms of the lowest achievable residual in model fitting. Specifically, SIME can achieve lower fitting residual than MC. However, it does not mean that SIME is superior over MC, since there exist applications where the task is simply to identify and remove outliers or the model is only secondary (e.g. the segmentation task). In light of this, SIME can be viewed as a valid alternative of MC.

3 Efficient Algorithms

Like the MC formulation, SIME (1) is also NP-hard, for which a global optimum can only be guaranteed by searching based algorithms. A natural scheme is to update the variables θ and s in an alternating manner. Since the problem is highly nonconvex involving binary variables, the direct AM algorithm can easily get trapped in local minima. In an attempt to mitigate this problem, we additionally propose an algorithm using SDR on the binary variable s .

3.1 Direct Alternating Minimization Algorithm

The AM algorithm solves (1) via alternately updating the model parameter θ and the binary slack variable s . First, fixing θ , the s -subproblem can be solved explicitly as

$$s_i = \begin{cases} 1, & \Phi(r_i(\theta)) > \beta \\ 0, & \Phi(r_i(\theta)) \leq \beta \end{cases}, \quad 1 \leq i \leq N. \quad (7)$$

Then, fixing s , the θ -subproblem is given by

$$\min_{\theta \in \mathbb{R}^d} \sum_{i=1}^N (1-s_i) \Phi(r_i(\theta)), \quad \text{s.t. } h(\theta) = 0, \quad (8)$$

which depends on the residual models of specific applications. We consider two main cases, linear or nonlinear residual model.

Case 1 (Linear residual). Linear residual model is widely used in MC [1], which typically has a form of

$$r_i(\theta) = |\mathbf{a}_i^T \theta - b_i|. \quad (9)$$

In robust linear regression and many computer vision applications, the residual $r_i(\boldsymbol{\theta})$ can be conveniently expressed in this form. As will be shown in Section 4, in homography, fundamental matrix, and affinity estimation in multi-view geometry under algebraic distance, the residual can be expressed in a linear form as (9). With linear residual model, if Φ is chosen as the ℓ_p loss, the model fitting term in SIME becomes

$$\Phi(r_i(\boldsymbol{\theta})) = |\mathbf{a}_i^T \boldsymbol{\theta} - b_i|^p. \quad (10)$$

For Gaussian inlier noise, $p = 2$ is the optimal choice, while for super-Gaussian inlier noise, the optimal value of p should be $p < 2$. Generally, a smaller p should be used when the inlier noise distribution has a thicker tail. Since the outliers are modeled as a wide uniform distribution (Proposition 1), it is reasonable to assume that the inlier noise is not too impulsive and hence we can restrict $p \geq 1$, in which case Φ is convex. When $p = 2$, the $\boldsymbol{\theta}$ -subproblem with or without the constraint $\|\boldsymbol{\theta}\| = 1$ can be solved explicitly. When $p \neq 2$, it can be solved by the reweighted LS algorithm, which is detailed in Appendix C.

Note that, even with quasi-convex geometric distance, deterministic MC algorithms usually use linear residual model, as both the ℓ_1 - and ℓ_∞ -norm reprojection residual under geometric distance can be linearized, e.g., in homography estimation and triangulation. However, we handle it in a different manner as presented in the following Case 2. Moreover, in rotation search, additional norm-one constraint appears under the linear residual model, which can also be solved explicitly when $p = 2$ as detailed in Section 4.3.

Case 2 (Nonlinear residual). Geometric distance based residual model is geometrically or statistically meaningful and, hence, is of more interest in practical applications than algebraic distance [37]. For many vision applications, the geometric residual functions have a generalized form as [37], [38]

$$r_i(\boldsymbol{\theta}) = \frac{\|\mathbf{U}_i \boldsymbol{\theta} + \mathbf{u}_i\|_p}{\mathbf{w}_i^T \boldsymbol{\theta} + w_i}, \quad \text{with } \mathbf{w}_i^T \boldsymbol{\theta} + w_i > 0, \quad (11)$$

where $p \geq 1$, $\mathbf{U}_i \in \mathbb{R}^{2 \times d}$, $\mathbf{u}_i \in \mathbb{R}^2$, and $\mathbf{w}_i \in \mathbb{R}^d$. In MC methods, linearization is usually used to handle such quasi-convex residual. For example, with a residual threshold of τ (in geometric unit such as pixel), the residual constraint can be expressed as

$$\|\mathbf{U}_i \boldsymbol{\theta} + \mathbf{u}_i\|_p \leq \tau(\mathbf{w}_i^T \boldsymbol{\theta} + w_i), \quad (12)$$

where $\mathbf{w}_i^T \boldsymbol{\theta} + w_i > 0$ is implicitly satisfied since $\tau > 0$ and $\|\mathbf{U}_i \boldsymbol{\theta} + \mathbf{u}_i\|_p \geq 0$. Then, for the two special cases of $p = 1$ or $p = \infty$, corresponding to the ℓ_1 - and ℓ_∞ -norm, respectively, (12) can be equivalently expressed as four linear inequalities.

Naturally, for SIME, we can use the squared ℓ_2 reprojection error as the individual loss, i.e.,

$$\Phi(r_i(\boldsymbol{\theta})) = \frac{\|\mathbf{U}_i \boldsymbol{\theta} + \mathbf{u}_i\|^2}{(\mathbf{w}_i^T \boldsymbol{\theta} + w_i)^2}. \quad (13)$$

Then, gradient descent based algorithm can be directly applied to update $\boldsymbol{\theta}$. Alternatively, the ℓ_∞ approach [39], [40] can be adopted, which minimizes the ℓ_∞ -norm of individual reprojection errors instead of the sum of their square. As the point-wise maximum (equivalently the ℓ_∞ -

Algorithm 1: AM Algorithm

Input: A start point $(\boldsymbol{\theta}_0, \mathbf{s}_0)$, and set $\beta > 0$.
 While not converged ($k = 0, 1, 2, \dots$) do
 Update \mathbf{s} by (7) for fixed $\boldsymbol{\theta}_k$ to obtain \mathbf{s}_{k+1} .
 Update $\boldsymbol{\theta}$ by (8) for fixed \mathbf{s}_{k+1} to obtain $\boldsymbol{\theta}_{k+1}$.
 End while
 Output: $(\boldsymbol{\theta}_{k+1}, \mathbf{s}_{k+1})$.

norm) of a set of quasi-convex functions is still quasi-convex, it does not have local minima. In comparison, the sum of quasi-convex functions (13) is no longer quasi-convex and can have multiple local minima. The algorithm is summarized as Algorithm 1.

3.2 Semidefinite Relaxation Based Algorithm

The direct AM algorithm is efficient, but can easily get trapped in local minima due to the high nonconvexity of (1), which involves binary variables. In an attempt to alleviate this problem, we consider a relaxation of the binary variables by SDR. SDR has been shown to be very effective in handling combinatorial problems, and it is tighter than linear relaxation [24], [25].

Let $\tilde{\mathbf{s}} \in \{-1, 1\}^{N+1}$, $\mathbf{S} = \tilde{\mathbf{s}}\tilde{\mathbf{s}}^T$, $\Phi_i := \Phi(r_i(\boldsymbol{\theta}))$, and

$$\mathbf{\Lambda} = \begin{bmatrix} 0 & (\beta - \Phi^T)/2 \\ (\beta - \Phi)/2 & \text{diag}(\Phi) \end{bmatrix},$$

with $\Phi = [\Phi_1, \Phi_2, \dots, \Phi_N]^T$. Then, problem (1) is equivalent to (proof is given in Appendix A)

$$\begin{aligned} & \min_{\boldsymbol{\theta} \in \mathbb{R}^d, \mathbf{S} \in \mathbb{S}^{(N+1)}} \text{tr}(\mathbf{\Lambda} \mathbf{S}) \\ & \text{s.t. } \text{diag}(\mathbf{S}) = \mathbf{1}_{N+1}, \mathbf{S} \succeq \mathbf{0}, \text{rank}(\mathbf{S}) = 1, h(\boldsymbol{\theta}) = 0. \end{aligned} \quad (14)$$

Then, dropping the rank-1 nonconvex constraint leads to a SDR of (1) as

$$\begin{aligned} & \min_{\boldsymbol{\theta} \in \mathbb{R}^d, \mathbf{S} \in \mathbb{S}^{(N+1)}} \text{tr}(\mathbf{\Lambda} \mathbf{S}) \\ & \text{s.t. } \text{diag}(\mathbf{S}) = \mathbf{1}_{N+1}, \mathbf{S} \succeq \mathbf{0}, h(\boldsymbol{\theta}) = 0. \end{aligned} \quad (15)$$

The above SDR is standard and widely used in binary combinatorial optimization problems [25], except that our problem additionally involves another variable $\boldsymbol{\theta}$ needing to be solved simultaneously. As a consequence, unlike most existing well-studied SDR problems resulting in convex relaxed formulations, problem (15) is nonconvex. However, for some applications with Φ and r_i being convex, problem (15) can be biconvex, which is detailed in Appendix B.

The problem (15) can be solved via alternatingly updating $\boldsymbol{\theta}$ and \mathbf{S} . Specifically, fixing \mathbf{S} , problem (15) becomes

$$\begin{aligned} & \min_{\boldsymbol{\theta} \in \mathbb{R}^d} \sum_{i=1}^N (1 - S_{1,i+1}) \Phi(r_i(\boldsymbol{\theta})) \\ & \text{s.t. } h(\boldsymbol{\theta}) = 0, \end{aligned} \quad (16)$$

which is a form of (8). Fixing $\boldsymbol{\theta}$, the \mathbf{S} -update subproblem becomes

$$\begin{aligned} & \min_{\mathbf{S} \in \mathbb{S}^{(N+1)}} \text{tr}(\mathbf{\Lambda} \mathbf{S}) \\ & \text{s.t. } \text{diag}(\mathbf{S}) = \mathbf{1}_{N+1}, \mathbf{S} \succeq \mathbf{0}. \end{aligned} \quad (17)$$

It is a standard SDP and can be solved by well-established SDP solvers, such as CVX [32]. But such solvers using prime-

dual interior algorithm have a complexity of $O((N+1)^{4.5})$ at the worst-case, and do not scale to moderate to large problem sizes.

In order to make the algorithm scalable to high dimension problems, the low-rank property of \mathbf{S} can be exploited by the Burer-Monteiro (B-M) factorization [25], e.g., using $\mathbf{S} = \mathbf{R}\mathbf{R}^T$ with $\mathbf{R} \in \mathbb{R}^{(N+1) \times p}$ to recast (17) into

$$\begin{aligned} \min_{\mathbf{R} \in \mathbb{R}^{(N+1) \times p}} \quad & \text{tr}(\mathbf{A}\mathbf{R}\mathbf{R}^T) \\ \text{s.t.} \quad & \text{diag}(\mathbf{R}\mathbf{R}^T) = \mathbf{1}_{N+1}. \end{aligned} \quad (18)$$

The B-M method is especially efficient to handle SDP problems, which has been applied in robotics and vision such as [56]. With this reformulation, the parameter number is reduced from $(N+1)^2$ to $p(N+1)$. It has been proven that there exists an optimum of (17) with rank less than $\lceil \sqrt{2N} \rceil$ [33, 25], hence using $p \geq \lceil \sqrt{2N} \rceil$ can guarantee that any optimum of (18) is also an optimum of (17). Meanwhile, although problem (18) is nonconvex, it almost never has any spurious local optima [34].

Proposition 4 [34]. For almost all \mathbf{A} , if $p(p+1) \geq 2(N+1)$, any local optimum \mathbf{R}^* of (18) is a global optimum of (18), and $\mathbf{R}^* \mathbf{R}^{*T}$ is a global optimum of (17).

This result implies that, despite the nonconvexity of (18), local optimization algorithms can converge to global optima. Accordingly, the first-order augmented Lagrangian algorithm [25] can be used. Rather than directly using this algorithm, we exploit the sparsity structure of the problem to achieve further acceleration. This is based on the fact that only the first column, first row and diagonal of \mathbf{A} have nonzero elements. Specifically, let $\mathbf{r}_i^T := \mathbf{R}(i, :)$ denote the i -th row of \mathbf{R} and $\mathbf{r} := [\mathbf{r}_1^T, \mathbf{r}_2^T, \dots, \mathbf{r}_{N+1}^T]^T \in \mathbb{R}^{p(N+1)}$, using the equivalence between $\text{diag}(\mathbf{R}\mathbf{R}^T) = \mathbf{1}_{N+1}$ and $\|\mathbf{r}_i\|^2 = 1$ for $1 \leq i \leq N+1$, problem (18) can be reformulated as an unconstrained problem

$$\min_{\mathbf{r} \in \mathbb{R}^{p(N+1)}} J(\mathbf{r}) := 2 \sum_{i=2}^{N+1} \Lambda_{1,i} \frac{\mathbf{r}_1^T \mathbf{r}_i}{\|\mathbf{r}_1\| \|\mathbf{r}_i\|} \quad (19)$$

where the norm-one constraints are removed by changing variable to $[\mathbf{R}(i, :)]^T = \mathbf{r}_i / \|\mathbf{r}_i\|$ [35], which leads to an unconstrained formulation.

Due to the equivalence between (18) and (19), and from Proposition 4, a local optimization algorithm can be employed to solve (19), and any solution satisfies first- and second-order necessary optimality conditions is a global optimum. Hence, any efficient first-order algorithm can be employed, e.g., the limited memory BFGS (L-BFGS) algorithm [36]. Such algorithms only require evaluating the first-order gradient of the objective, which is

$$\nabla_{\mathbf{r}} J(\mathbf{r}) = \left[\nabla_{\mathbf{r}_1^T} J(\mathbf{r}), \nabla_{\mathbf{r}_2^T} J(\mathbf{r}), \dots, \nabla_{\mathbf{r}_{N+1}^T} J(\mathbf{r}) \right]^T,$$

with

$$\begin{aligned} \nabla_{\mathbf{r}_1} J(\mathbf{r}) &= 2 \sum_{i=2}^{N+1} \Lambda_{1,i} \frac{\|\mathbf{r}_1\|^2 \mathbf{r}_i - \mathbf{r}_1^T \mathbf{r}_i \mathbf{r}_1}{\|\mathbf{r}_1\|^3 \|\mathbf{r}_i\|}, \\ \nabla_{\mathbf{r}_i} J(\mathbf{r}) &= 2 \Lambda_{1,i} \frac{\|\mathbf{r}_i\|^2 \mathbf{r}_1 - \mathbf{r}_1^T \mathbf{r}_i \mathbf{r}_i}{\|\mathbf{r}_1\| \|\mathbf{r}_i\|^3}, \quad \text{for } 2 \leq i \leq N+1. \end{aligned}$$

Algorithm 2: AM Algorithm with SDR (AM-R)

Input: A start point $(\boldsymbol{\theta}_0, \mathbf{S}_0)$, and set $\beta > 0$.
 While not converged ($k = 0, 1, 2, \dots$) do
 Update \mathbf{S} by (17) for fixed $\boldsymbol{\theta}_k$ to obtain \mathbf{S}_{k+1} .
 Update $\boldsymbol{\theta}$ by (16) for fixed \mathbf{S}_{k+1} to obtain $\boldsymbol{\theta}_{k+1}$.
 End while
 Output: $(\boldsymbol{\theta}_{k+1}, \mathbf{S}_{k+1})$.

4 Applications

This section presents the applications of SIME, mainly include projective transformation estimation in multi-view geometry under algebraic or geometric distance, rotation search, and 6-DoF rigid registration. Projective transformations and projections constitute a cornerstone of modern vision geometry [37]. Rotation search, also known as the Wahba problem, aims to estimate the rotation between two coordinate frames, which has wide applications in computer vision, robotics, and aerospace engineering [42]–[46]. 6-DoF rigid registration can be viewed as an extension of 3-DoF rotation search, which estimates both rotation and translation.

4.1 Projective Transformation Estimation with Algebraic Distance

This subsection applies SIME to homography, fundamental matrix and affinity estimation under algebraic distance. For all these problems, the set of correspondences from two views are denoted by $\{(\mathbf{x}_i, \mathbf{x}'_i) : \mathbf{x}_i \leftrightarrow \mathbf{x}'_i, i = 1, 2, \dots, N\}$ with $\mathbf{x}_i, \mathbf{x}'_i \in \mathbb{P}^2$. Meanwhile, $\tilde{\mathbf{x}}_i = [\mathbf{x}_i^T \ 1]^T$ and $\tilde{\mathbf{x}}'_i = [\mathbf{x}'_i^T \ 1]^T$ are the homogeneous representation.

Homography arises in plane-to-plane mapping. The problem is to compute a matrix $\mathbf{H} \in \mathbb{R}^{3 \times 3}$ such that $\tilde{\mathbf{x}}_i = \mathbf{H} \tilde{\mathbf{x}}'_i$ for inliers. The matrix \mathbf{H} has 8 DoF and is only defined up to scale. Accordingly, it can be conveniently defined as

$$\mathbf{H} = \begin{bmatrix} h_1 & h_2 & h_3 \\ h_4 & h_5 & h_6 \\ h_7 & h_8 & 1 \end{bmatrix}.$$

Denote $\boldsymbol{\theta} = [h_1, h_2, \dots, h_8]^T \in \mathbb{R}^8$, homography estimation with algebraic distance can be expressed in a linear form as [37]

$$\mathbf{A}\boldsymbol{\theta} = \mathbf{b}, \quad (20)$$

where $\mathbf{A} = [\mathbf{a}_1, \dots, \mathbf{a}_N]^T$ and $\mathbf{b} = [b_1, \dots, b_N]^T$ are determined by $\{(\mathbf{x}_i, \mathbf{x}'_i) : i = 1, 2, \dots, N\}$. With this expression, linear residual model is usually used in MC as (9). Using linear residual and with Φ being the ℓ_p loss, the model fitting term in SIME conforms to (10).

Fundamental matrix is the algebraic representation of intrinsic projective geometry between two views. The problem is to compute a matrix $\mathbf{F} \in \mathbb{R}^{3 \times 3}$ such that $\tilde{\mathbf{x}}_i^T \mathbf{F} \tilde{\mathbf{x}}'_i = 0$ for inliers. Though the reprojection error is neither linear nor quasi-convex, the epipolar constraint $\tilde{\mathbf{x}}_i^T \mathbf{F} \tilde{\mathbf{x}}'_i = 0$ can be linearized to have a form of (20) with $\boldsymbol{\theta} = \text{vec}(\mathbf{F}) \in \mathbb{R}^9$ [37].

Affinity estimation also admits a linear residual model, in which the geometric matching error for the i -th correspondence is

$$r_i(\boldsymbol{\theta}) = \|\mathbf{x}_i - \boldsymbol{\theta} \tilde{\mathbf{x}}'_i\|_1,$$

where $\Theta \in \mathbb{R}^{2 \times 3}$ stands for the affine transformation, and $\theta = \text{vec}(\Theta) \in \mathbb{R}^6$. This residual can be split into two terms, which also conforms to (9). Particularly, for affine transformation, geometric and algebraic distances are identical.

4.2 Projective Transformation Estimation with Geometric Distance

While algebraic distance is convenient due to its linearity, geometric distance is geometrically or statistically meaningful. Interested application examples include homography estimation and triangulation. For homography estimation, the geometric residual is given by

$$r_i(\theta) = \frac{\|[\mathbf{h}_1, \mathbf{h}_2]^T \tilde{\mathbf{x}}'_i - \mathbf{h}_3^T \tilde{\mathbf{x}}'_i\|_p}{\mathbf{h}_3^T \tilde{\mathbf{x}}'_i},$$

where \mathbf{h}_k^T is the k -th row of \mathbf{H} and $\theta = \text{vec}(\mathbf{H})$. Given multi-view observations of 3D points with known camera matrices, the triangulation problem is to estimate the 3D points that project to the given image points. For triangulation, for each image point \mathbf{x}_i and camera matrix $\mathbf{P}_i \in \mathbb{R}^{3 \times 4}$, the reprojection error of the point estimation $\theta \in \mathbb{R}^3$ is

$$r_i(\theta) = \frac{\|([\mathbf{p}_1^i, \mathbf{p}_2^i]^T - \mathbf{x}_i \mathbf{p}_3^i)^T \tilde{\theta}\|_p}{\mathbf{p}_3^i \tilde{\theta}},$$

where \mathbf{p}_k^i is the k -th row of \mathbf{P}_i and $\tilde{\theta} = [\theta^T \ 1]^T$. In both the applications with geometric distance, the residual have a form of (11), and the proposed algorithm can be applied.

4.3 Rotation Search

Consider a set of 3D point pairs $\{(\mathbf{a}_i, \mathbf{b}_i) : i = 1, 2, \dots, N\}$ with $\mathbf{a}_i, \mathbf{b}_i \in \mathbb{R}^3$, which are generated as

$$\mathbf{b}_i = \mathbf{R}\mathbf{a}_i + \mathbf{n}_i + \mathbf{o}_i, \quad (21)$$

where $\mathbf{R} \in \text{SO}(3)$ is the unknown rotation, \mathbf{n}_i models small inlier measurement noise, \mathbf{o}_i is zero if the data pair $(\mathbf{a}_i, \mathbf{b}_i)$ is inlier, or \mathbf{o}_i is an arbitrary perturbation if $(\mathbf{a}_i, \mathbf{b}_i)$ is outlier.

For convenience, we adopt quaternion representation for 3D rotation [47]. Denote a unit quaternion by $\mathbf{q} = [\mathbf{v}^T \ s]^T$, where $\mathbf{v} \in \mathbb{R}^3$ is the vector part and s is the scalar part. If \mathbf{R} is the unique rotation corresponding to a unit quaternion \mathbf{q} , then the rotation of a vector $\mathbf{a} \in \mathbb{R}^3$ by \mathbf{R} can be expressed in terms of quaternion product as

$$\begin{bmatrix} \mathbf{R}\mathbf{a} \\ 0 \end{bmatrix} = \mathbf{q} \circ \hat{\mathbf{a}} \circ \mathbf{q}^{-1},$$

where $\mathbf{q}^{-1} = [-\mathbf{v}^T \ s]^T$ is the quaternion inverse, and $\hat{\mathbf{a}} = [\mathbf{a}^T \ 0]^T$. The quaternion product is defined as $\mathbf{q} \circ \mathbf{x} = \Omega(\mathbf{q})\mathbf{x}$ for any $\mathbf{x} \in \mathbb{R}^4$, and $\mathbf{q}_1 \circ \mathbf{q}_2 = \Omega(\mathbf{q}_1)\mathbf{q}_2 = \bar{\Omega}(\mathbf{q}_2)\mathbf{q}_1$ for two unit quaternion \mathbf{q}_1 and \mathbf{q}_2 , where

$$\Omega(\mathbf{q}) = \begin{bmatrix} q_4 & -q_3 & q_2 & q_1 \\ q_3 & q_4 & -q_1 & q_2 \\ -q_2 & q_1 & q_4 & q_3 \\ -q_1 & -q_2 & -q_3 & q_4 \end{bmatrix}, \quad \bar{\Omega}(\mathbf{q}) = \begin{bmatrix} q_4 & q_3 & -q_2 & q_1 \\ -q_3 & q_4 & q_1 & q_2 \\ q_2 & -q_1 & q_4 & q_3 \\ -q_1 & -q_2 & -q_3 & q_4 \end{bmatrix}.$$

Based on quaternion representation, the linear residual with a LS loss can be expressed as

$$\Phi(r_i(\theta)) = \|\hat{\mathbf{b}}_i - \theta \circ \hat{\mathbf{a}}_i \circ \theta^{-1}\|^2, \quad \text{with } \|\theta\| = 1. \quad (22)$$

For the AM-R algorithm, similar to (15), the SDR of SIME in this case leads to

$$\begin{aligned} & \min_{\theta \in \mathbb{R}^4, \mathbf{S} \in \mathbb{S}^{(N+1)}} \text{tr}(\Lambda \mathbf{S}) \\ & \text{s.t. } \text{diag}(\mathbf{S}) = \mathbf{1}_{N+1}, \mathbf{S} \succeq \mathbf{0}, \|\theta\| = 1. \end{aligned} \quad (23)$$

Accordingly, the θ -subproblem becomes

$$\begin{aligned} & \min_{\theta \in \mathbb{R}^4} \sum_{i=1}^N (1 - S_{1,i+1}) \|\hat{\mathbf{b}}_i - \theta \circ \hat{\mathbf{a}}_i \circ \theta^{-1}\|^2 \\ & \text{s.t. } \|\theta\| = 1. \end{aligned} \quad (24)$$

For a unit quaternion θ , it follows that $c = \theta^T (c\mathbf{I}_4)\theta$ for any $c \in \mathbb{R}$, $\hat{\mathbf{b}}_i^T(\theta \circ \hat{\mathbf{a}}_i \circ \theta^{-1}) = \theta^T \Omega^T(\hat{\mathbf{b}}_i) \bar{\Omega}(\hat{\mathbf{a}}_i) \theta$ and $-\Omega^T(\hat{\mathbf{b}}_i) = \Omega(\hat{\mathbf{b}}_i)$, hence problem (24) can be rewritten as

$$\min_{\theta \in \mathbb{R}^4} \theta^T \mathbf{G} \theta, \quad \text{s.t. } \|\theta\| = 1, \quad (25)$$

with

$$\mathbf{G} = \sum_{i=1}^N (1 - S_{1,i+1}) \left[(\|\mathbf{b}_i\|^2 + \|\mathbf{a}_i\|^2) \mathbf{I}_4 + 2\Omega(\hat{\mathbf{b}}_i) \bar{\Omega}(\hat{\mathbf{a}}_i) \right].$$

Obviously, the solution of (25) is given by the eigenvector corresponding to the smallest eigenvalue of \mathbf{G} .

Next, we compare the proposed method with a close existing method [31], namely QUASAR (QUATernion-based Semidefinite relAXation for Robust alignment). QUASAR uses a truncated LS loss and has a formulation as

$$\min_{\substack{\theta \in \mathbb{R}^4, \|\theta\|=1 \\ s_i \in \{-1, 1\}}} \sum_{i=1}^N \frac{1 - s_i}{2} \frac{\|\hat{\mathbf{b}}_i - \theta \circ \hat{\mathbf{a}}_i \circ \theta^{-1}\|^2}{\sigma^2} + \frac{1 + s_i}{2} \bar{c}^2, \quad (26)$$

which can be viewed as a special instance of the SIME formulation. To solve this mixed-integer program, QUASAR adopts a binary cloning based reformulation as

$$\begin{aligned} & \min_{\substack{\theta \in \mathbb{R}^4, \|\theta\|=1 \\ \theta_i = \pm \theta}} \sum_{i=1}^N \frac{\|\hat{\mathbf{b}}_i - \theta \circ \hat{\mathbf{a}}_i \circ \theta^{-1} - \theta^T \theta_i \hat{\mathbf{b}}_i + \theta \circ \hat{\mathbf{a}}_i \circ \theta_i^{-1}\|^2}{4\sigma^2} \\ & \quad + \frac{1 + \theta^T \theta_i}{2} \bar{c}^2. \end{aligned} \quad (27)$$

This reformulation is based on the fact that, if $\theta_i = s_i \theta$ with $s_i \in \{-1, 1\}$, then $\theta^T \theta_i = s_i$ and $\theta \circ \hat{\mathbf{a}}_i \circ \theta_i^{-1} = s_i(\theta \circ \hat{\mathbf{a}}_i \circ \theta^{-1})$. Let $\tilde{\theta} = [\theta^T, \theta_1^T, \dots, \theta_N^T]^T$, problem (27) can be expressed as [31]

$$\begin{aligned} & \min_{\tilde{\theta} \in \mathbb{R}^{4(N+1)}} \tilde{\theta}^T \mathbf{Q} \tilde{\theta} \\ & \text{s.t. } \|\theta\| = 1, \theta_i \theta_i^T = \theta \theta^T, \forall i = 1, \dots, N, \end{aligned} \quad (28)$$

where $\mathbf{Q} \in \mathbb{R}^{4(N+1) \times 4(N+1)}$ is given by

$$\mathbf{Q} = \begin{bmatrix} \mathbf{0} & \mathbf{Q}_{01} & \dots & \mathbf{Q}_{0N} \\ \mathbf{Q}_{01}^T & \mathbf{Q}_{11} & \dots & \mathbf{0} \\ \vdots & \vdots & \ddots & \vdots \\ \mathbf{Q}_{0N}^T & \mathbf{0} & \dots & \mathbf{Q}_{NN} \end{bmatrix},$$

with

$$\mathbf{Q}_{ii} = \frac{(\|\mathbf{b}_i\|^2 + \|\mathbf{a}_i\|^2) \mathbf{I}_4 + 2\Omega(\hat{\mathbf{b}}_i) \bar{\Omega}(\hat{\mathbf{a}}_i)}{2\sigma^2} + \frac{\bar{c}^2}{2} \mathbf{I}_4,$$

$$\mathbf{Q}_{0i} = -\frac{(\|\mathbf{b}_i\|^2 + \|\mathbf{a}_i\|^2)\mathbf{I}_4 + 2\Omega(\hat{\mathbf{b}}_i)\bar{\Omega}(\hat{\mathbf{a}}_i)}{4\sigma^2} + \frac{\bar{c}^2}{4}\mathbf{I}_4.$$

Then, let $\mathbf{Z} = \tilde{\boldsymbol{\theta}}\tilde{\boldsymbol{\theta}}^T \in \mathbb{S}^{4(N+1)}$ and denote its 4×4 sub-blocks by $[\mathbf{Z}]_{ij} = \boldsymbol{\theta}_i\boldsymbol{\theta}_j^T$ for $\forall 0 \leq i, j \leq N$ with $\boldsymbol{\theta}_0 = \boldsymbol{\theta}$, QUASAR adopts a SDR of (28) as

$$\begin{aligned} & \min_{\mathbf{Z} \in \mathbb{S}^{4(N+1)}} \text{tr}(\mathbf{Q}\mathbf{Z}) \\ \text{s.t. } & \text{tr}([\mathbf{Z}]_{00}) = 1, \mathbf{Z} \succeq \mathbf{0}, \\ & [\mathbf{Z}]_{ii} = [\mathbf{Z}]_{00}, \forall i = 1, \dots, N, \\ & [\mathbf{Z}]_{ij} = [\mathbf{Z}]_{ij}^T, \forall 0 \leq i < j \leq N. \end{aligned} \quad (29)$$

The next result compares QUASAR with the proposed AM-R algorithm (proof see Appendix D).

Proposition 5. If the SIME formulation uses the loss (22) and with $\beta = \sigma^2\bar{c}^2$, then it is equivalent to the QUASAR formulations (26)–(28). Furthermore, the relaxation (23) of SIME is tighter than the relaxation (29) of QUASAR.

Remark 4 (Computational complexity). It has been shown in [31] that the relaxation (29) with redundant constraints is sufficiently tight. Particularly, in the noiseless and outlier-free case, it is always tight as its optimal solution has rank-1 and attains a global minimum of the original nonconvex problem. However, QUASAR solving (29) is computationally expensive and scales poorly in problem size. For example, with a general SDP solver it typically needs more than 1000 seconds for $N = 100$ [31]. Although (29) is also a SDP like the \mathbf{S} -subproblem (17), the accelerating procedure in Section 3.2 does not apply to it. That is because the SDP (29) involves a large number of equality constraints, about $3N^2 + 13N$. Meanwhile, the constraints do not admit an unconstrained formulation. Hence, when using the augmented Lagrangian method, a large number of dual variables (about $3N^2 + 13N$) have to be handled, which fundamentally increases the computational complexity. In comparison, (17) only has $N + 1$ equality constraints and, more importantly, the norm-one constraints have a special “hidden convexity” structure admitting an unconstrained formulation (19). This leads to a significant advantage of our algorithm over QUASAR in computational efficiency, e.g., three orders of magnitude faster as will be shown in Section 5.6.

Moreover, for the AM algorithm, the $\boldsymbol{\theta}$ -subproblem can be expressed as (24) with $(1 - S_{1,i+1})$ replaced by $(1 - s_i)$, where s_i is computed by (7).

4.4 6-DoF Euclidean Registration

In the context of 6-DoF Euclidean registration defined by a rigid transformation $[\mathbf{R}, \mathbf{t}] \in \mathbb{R}^{3 \times 4}$, where $\mathbf{R} \in \text{SO}(3)$ and \mathbf{t} are the unknown rotation and translation, respectively, the generation model (21) is extended to

$$\mathbf{b}_i = \mathbf{R}\mathbf{a}_i + \mathbf{t} + \mathbf{n}_i + \mathbf{o}_i. \quad (30)$$

In this case, using quaternion representation for rotation and with the LS loss, the fitting objective becomes

$$\Phi(r_i(\boldsymbol{\theta})) = \|\hat{\mathbf{b}}_i - \boldsymbol{\theta} \circ \hat{\mathbf{a}}_i \circ \boldsymbol{\theta}^{-1} - \hat{\mathbf{t}}\|^2, \text{ with } \|\boldsymbol{\theta}\| = 1, \quad (31)$$

where $\hat{\mathbf{t}} = [\mathbf{t}^T \ 0]^T$. Accordingly, the $\boldsymbol{\theta}$ -subproblem becomes

$$\begin{aligned} & \min_{\boldsymbol{\theta} \in \mathbb{R}^4, \mathbf{t} \in \mathbb{R}^3} \sum_{i=1}^N \omega_i \|\hat{\mathbf{b}}_i - \boldsymbol{\theta} \circ \hat{\mathbf{a}}_i \circ \boldsymbol{\theta}^{-1} - \hat{\mathbf{t}}\|^2 \\ \text{s.t. } & \|\boldsymbol{\theta}\| = 1. \end{aligned} \quad (32)$$

For the AM algorithm, $\omega_i = 1 - s_i$ with s_i be computed by (7), whilst for the AM-R algorithm, $\omega_i = 1 - S_{1,i+1}$ with $S_{i,j}$ be computed by (17). Then, the closed-form solution to problem (32) is given in [55].

5 Experimental Results

We evaluate the proposed algorithms in various 2D/3D registration experiments, including robust linear regression, homography estimation, affinity estimation, 3-DoF rotation registration, and 6-DoF Euclidean registration. The experiments are conducted on a desktop PC with a 3.4 GHz CPU and 32 GB RAM. For the AM-R algorithm (Algorithm 2), we set $p = \lceil \sqrt{2N}/3 \rceil$ for the low-rank factorization (18) and solve (19) by L-BFGS using minFunc [54].

5.1 Comparison between the AM and AM-R Algorithms

We first compare the two proposed algorithms to examine the effectiveness of the relaxation strategy. As discussed in Section 3, both the direct AM and the AM-R algorithms are local optimization algorithms, hence their performance are closely related to initialization. Fig. 1 compares their performance in two tasks with different initialization methods. The first is robust linear regression (experimental setting see Section 5.2) with random, Huber, L1 and RANSAC initialization. The second is rotation registration (experimental setting see Section 5.5) with random, Huber, GORE and RANSAC initialization. While RANSAC is randomized, Huber, L1, and GORE are deterministic methods. Particularly, GORE [50] can achieve guaranteed outlier removal and provide a rough estimation of the model from the pruned data. Each result is an average of 50 independent runs.

Clearly, for linear regression, different initialization yield similar performance of the two algorithms. However, for rotation registration, AM-R achieves distinctly better performance in the case of random, Huber and GORE initialization, which demonstrates the effectiveness of the SDR strategy. Compared with the linear regression task, the rotation registration task involves additional nonconvex constraint, e.g., $\|\boldsymbol{\theta}\| = 1$. In both cases, AM-R can perform satisfactorily with a proper initialization, e.g., with Huber, L1 or RANSAC initialization in linear regression, and with Huber, GORE or RANSAC initialization in rotation registration. Fig. 2 compares the average runtime of AM and AM-R, which includes the runtime of the initialization methods. As expected, the direct AM algorithm is much faster than AM-R.

5.2 Robust Linear Regression

This experiment considers the robust linear regression problem using synthetic data. The compared algorithms include RANSAC and three deterministic algorithms, the exact penalty method (EP) [21], the L1 method [17], and the iteratively reweighted (IRW) method [18]. A confidence

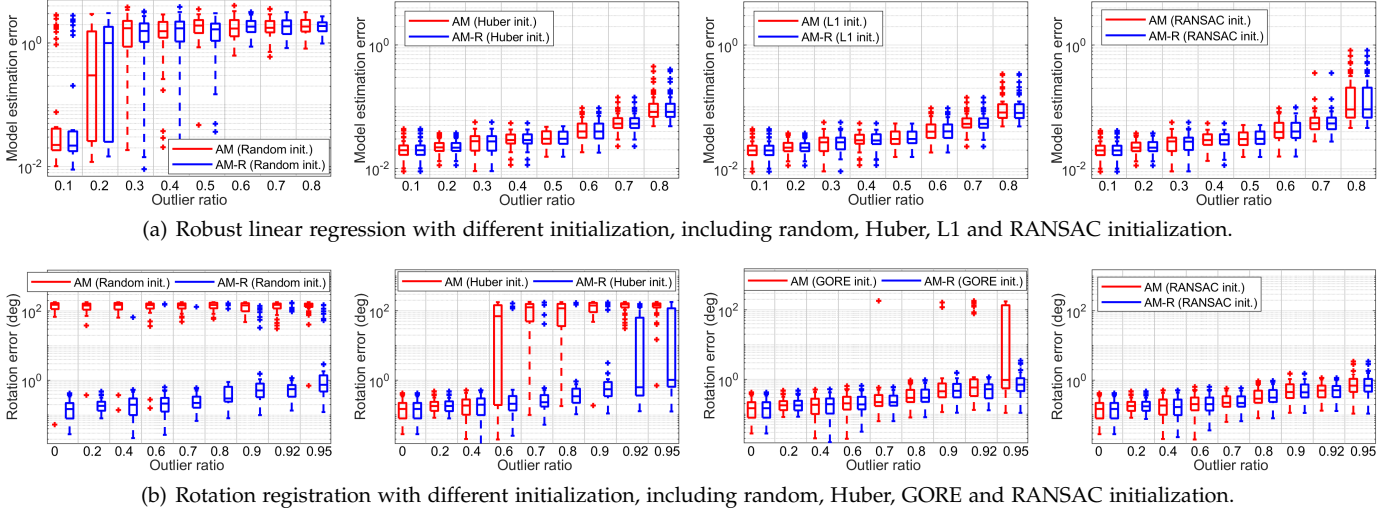


Fig. 1. Comparison between the AM and AM-R algorithms for different initialization methods, (a) Model estimation error versus outlier ratio in the linear regression experiment with $N = 250$, (b) Rotation error versus outlier ratio in the rotation registration experiment with $N = 100$.

$\rho = 0.99$ is used in the stopping criterion of RANSAC. For the EP algorithm, we use default parameters of it and employ Gurobi to solve the LP subproblems. Moreover, EP, AM and AM-R are initialized by the solution of the L1 method, and their runtime results include the runtime of the initialization. We generate N data points $\{\mathbf{a}_i, b_i\}_{i=1, \dots, N}$ as

$$b_i = \mathbf{a}_i^T \boldsymbol{\theta} + n_i + o_i,$$

where $\mathbf{a}_i, \boldsymbol{\theta} \in \mathbb{R}^8$, n_i is Gaussian noise with standard deviation of 0.1. o_i is zero if the data pair (\mathbf{a}_i, b_i) is inlier, or o_i is large perturbation if (\mathbf{a}_i, b_i) is outlier. A randomly selected subset of $\{b_i\}_{i=1, \dots, N}$ is corrupted by such high noise to simulate outliers. The elements of \mathbf{a}_i are randomly distributed in $[-1, 1]$.

Both AM and AM-R use the ℓ_2 loss (10). The inlier threshold τ for the RANSAC, EP, L1 and IRW methods is chosen to bound the inlier residual with a probability of 99.9%, i.e., $\mathbb{P}((b_i - \mathbf{a}_i^T \boldsymbol{\theta})^2 \leq \tau^2) = 1 - 10^{-3}$ for inliers. Under Gaussian noise, it can be computed from the 1-DoF Chi-squared distribution. For AM and AM-R, we choose $\beta = \Phi(\tau) = \tau^2$. Hence, the inlier thresholds for all the compared algorithms are the same. Since the estimation of $\boldsymbol{\theta}$ by an MC algorithm is only a feasible solution under inlier residual constraint, we compute a refined LS estimation for each MC algorithm based on its output inliers. This refinement is consistent with the LS fitting of AM and AM-R (with Φ be the LS loss), which makes the comparison fair. The refinement variants are referred to as RANSAC-r, EP-r, L1-r, and IRW-r.

Fig. 3 shows the estimation error of the algorithms versus outlier ratio for $N = 250$ in two outlier conditions, uniformly distributed in $[-2, 2]$ or Gaussian distributed with standard deviation of 2. Given an estimation $\hat{\boldsymbol{\theta}}$, the estimation error is defined as $\|\hat{\boldsymbol{\theta}} - \boldsymbol{\theta}\|/\|\boldsymbol{\theta}\|$. Each result is an average of 50 independent runs. It can be seen that the second-step refinement of each MC method yields much more accurate estimation than the original feasible solution. AM and AM-R distinctly outperforms the compared algorithms when the outlier ratio exceeds 20%. Its super-

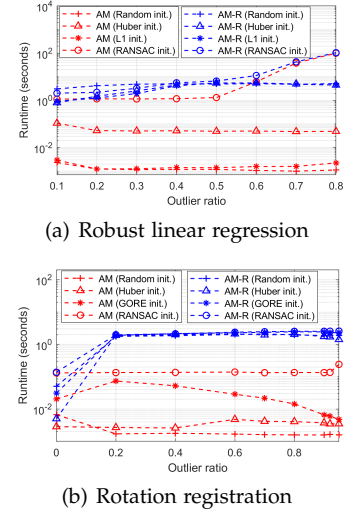


Fig. 2. Average runtime of AM and AM-R for different initialization methods, (a) Robust linear regression, (b) Rotation registration.

riority gets more prominent as the outlier ratio increases, and shows significantly better accuracy than the others at moderate to high outlier ratios. This advantage comes from that the SIME formulation (1) takes the fitting residual into consideration in identifying the inliers, while the MC methods do not.

Fig. 4 compares the consensus size and runtime in the case of uniformly distributed outliers. EP, AM and AM-R have similar consensus size. As shown in Proposition 2, the consensus size of an optimum SIME solution is theoretically upper bounded by that of an optimum MC solution. In terms of runtime, the L1 method is the fastest, while AM-R is much slower than L1, EP, IRW and AM. As expected, the runtime of RANSAC increases dramatically at high outlier ratios.

5.3 Homography Estimation with Algebraic Distance

This experiment considers homography estimation under algebraic residual model. The homography constraints

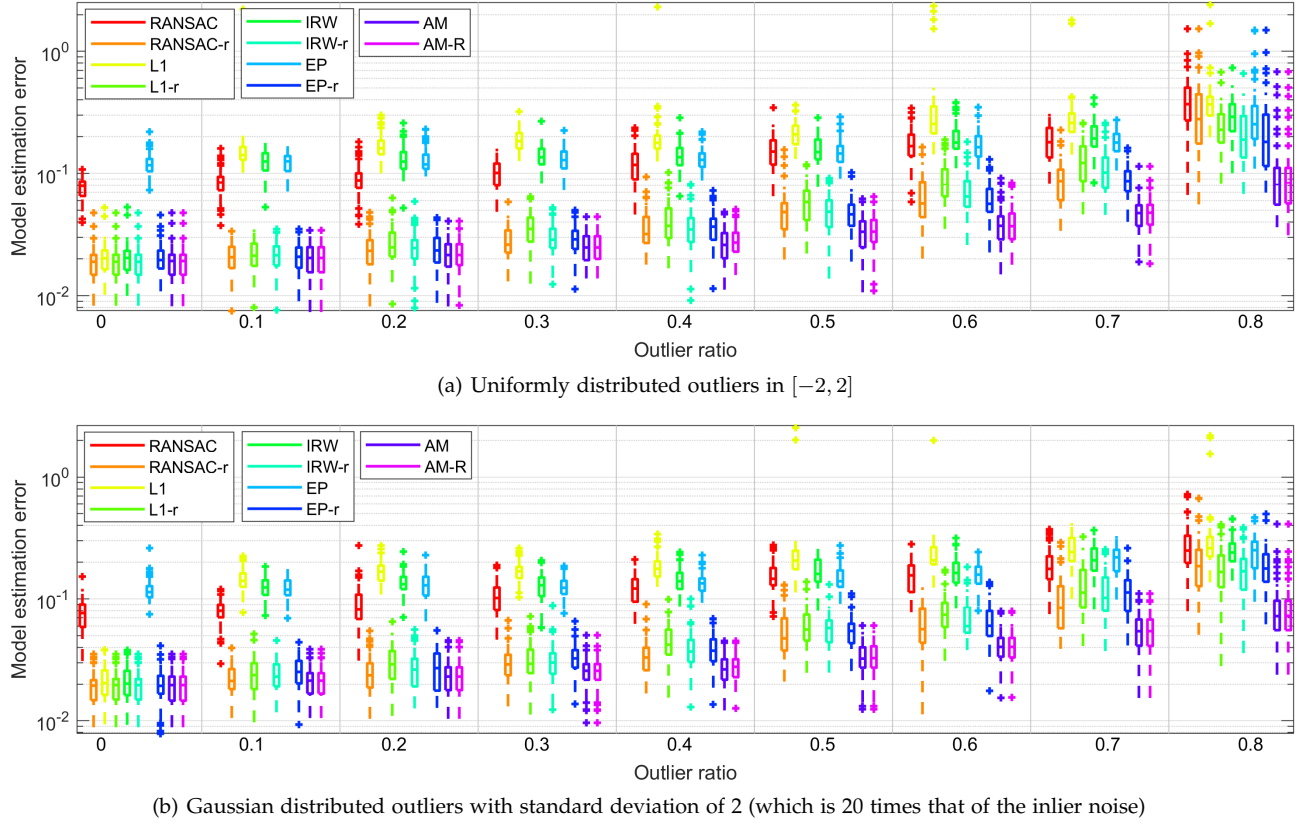


Fig. 3. Model estimation error versus outlier ratio in the linear regression experiment with $N = 250$. (a) Uniformly distributed outliers in $[-2, 2]$. (b) Gaussian distributed outliers with standard deviation of 2.

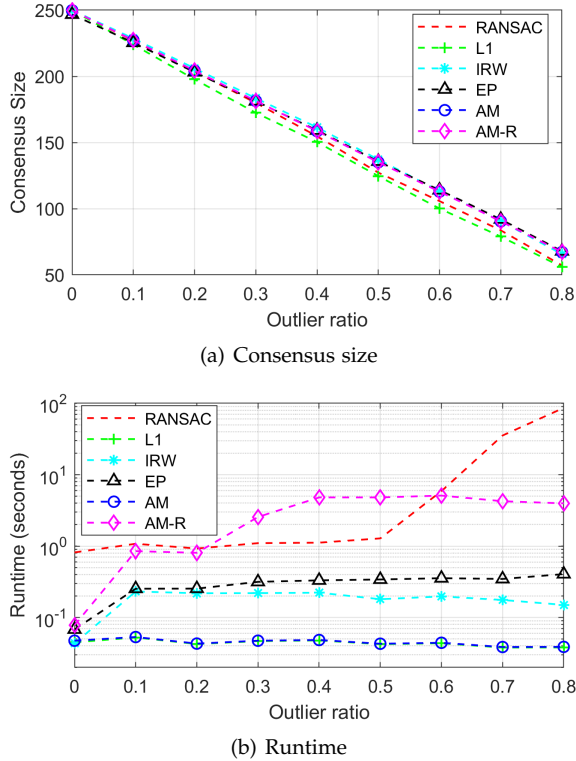


Fig. 4. Consensus size and runtime comparison in the linear regression experiment with uniformly distributed outliers in $[-2, 2]$. (a) Consensus size. (b) Runtime.

are linearized as [37, Chapter 4]. We use 20 pairs of images from the VGG dataset (Aerial views I, Corridor, Kapel, Merton II, Merton III, Valbonne Church, Boat, Bark, Bikes, Graff, Trees) and Zurich Building dataset (Building 4, 5, 22, 24, 28, 37, 59, 67, 199). The VLFeat toolbox [48] is employed to extract SIFT features and correspondence matching for each image pair. For the MC algorithms, the inlier threshold is set to $\tau = 0.5$, and accordingly for SIME we set $\beta = \Phi(\tau) = \tau^2$. EP, AM and AM-R are initialized by the L1 method.

Since the ground-truth transformation is unknown, we resort to compute a score for the estimated homography based on the symmetric transfer errors [37]. Specifically, with correspondences $\{(\mathbf{x}_i, \mathbf{x}'_i) : i = 1, 2, \dots, N\}$ and a homography \mathbf{H} , the score is computed as

$$S(\mathbf{H}) = \sum_i \rho(d^2(\mathbf{x}_i, \mathbf{H}\mathbf{x}'_i)) + \rho(d^2(\mathbf{x}'_i, \mathbf{H}^{-1}\mathbf{x}_i)), \quad (33)$$

where d^2 is the transfer error and

$$\rho(d^2) = \begin{cases} T - d^2, & \text{if } d^2 < T \\ 0, & \text{if } d^2 \geq T \end{cases},$$

with T being the outlier rejection threshold based on the 2-DoF χ^2 test at probability of 99% under the assumption that the measurement noise has a standard deviation of 1 pixel. A higher score implies a better estimation of the model, which is usually used to evaluate the quality of an estimated model in practice [49].

Fig. 5 shows the results of the algorithms on the 20 image pairs, including the score computed as (33), consensus

TABLE 1
Average score of homography estimation on 20 image pairs with algebraic distance.

RANSAC/ RANSAC-r	L1/L1-r	IRW/IRW-r	EP/EP-r	AM	AM-R
527/6183	12/5870	11/5797	64/6130	6416	6416

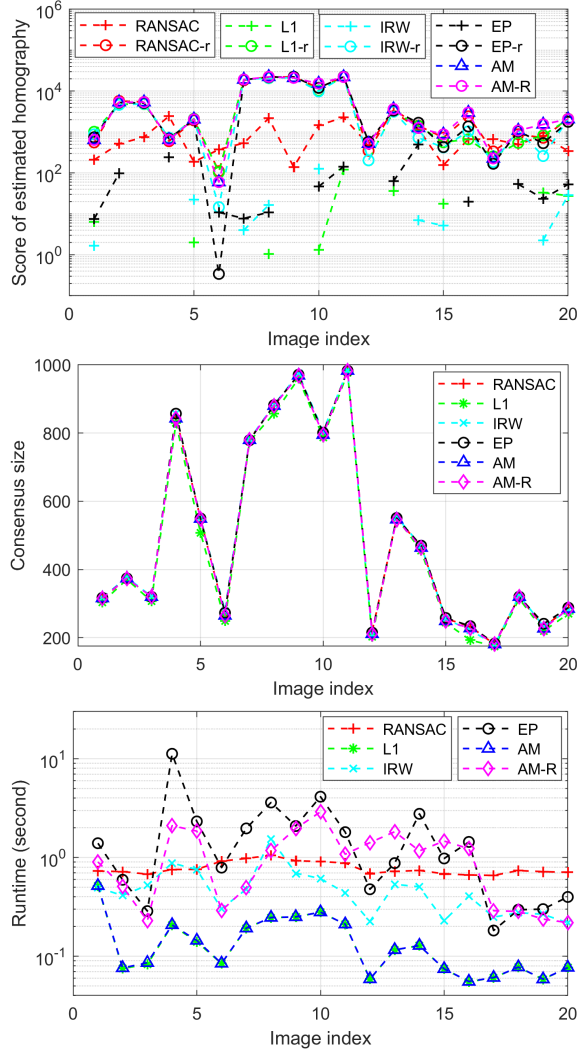
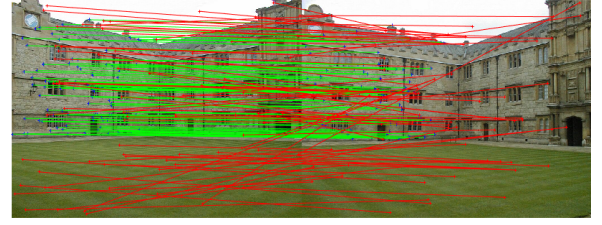


Fig. 5. Homography estimation results on 20 image pairs with algebraic distance. From top to bottom are respectively the score of estimated homography, consensus size, and runtime.

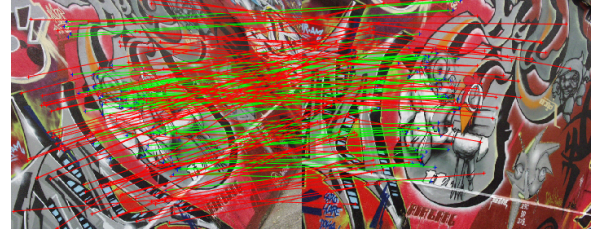
size, and runtime. Table 1 shows the average score of estimated homography on the 20 image pairs. Again, it can be observed that, for the four MC algorithms, the second-step refinement helps to attain significant better estimation. AM and AM-R achieve the highest average score. Fig. 6(a) presents some sample qualitative results of AM.

5.4 Homography Estimation with Geometric Distance

We further consider homography estimation under geometric residual model. For the MC methods, the residual constraint (12) with ℓ_1 -norm is used with a linearization. For AM and AM-R, the loss (13) is used. It has been shown in [39] that the ℓ_2 and ℓ_∞ methods generally have very similar performance in homography estimation with



(a) Homography estimation



(b) Affinity estimation

Fig. 6. Sample qualitative results of AM, (a) homography estimation, (b) affinity estimation. Red and green lines represent identified inliers and outliers, respectively (only 100 inliers/outliers are displayed for clarity).

TABLE 2
Average score of homography estimation on 20 image pairs with geometric distance.

RANSAC/ RANSAC-r	L1/L1-r	IRW/IRW-r	EP/EP-r	AM	AM-R
8135/ 8706	5709/ 7656	7202/ 8050	7644/ 8515	8801	8773

geometric distance. The inlier threshold is set to $\tau = 4$ pixels for the MC methods, while $\beta = \tau^2$ is used for SIME. EP, AM and AM-R are initialized by RANSAC, as it can yield better performance than L1 initialization in this experiment. We use the same data as the last experiment.

Fig. 7 presents the results of the algorithms on the 20 image pairs, including the score computed as (33), consensus size, and runtime. Table 2 shows the average score of estimated homography over the 20 image pairs. It can be seen that under geometric distance, the second-step refinement of the MC methods also helps to attain distinctly better accuracy. Noteworthy, AM achieves the highest score on 12 image pairs, while gives the largest consensus size on 18 image pairs. It is worth noting that, from Proposition 2, the consensus size of an optimum SIME solution is upper bounded by that of an optimum MC solution. However, as both the problems are nonconvex binary optimization problems, none of the compared algorithms is guaranteed to find an optimum solution. Hence, the larger consensus size of AM and AM-R demonstrates that the proposed algorithms are more effective. From Table 1 and 2, for all the compared methods, geometric distance yields significantly higher scores than algebraic distance. Moreover, AM achieves the highest average score.

5.5 Affinity Estimation

As introduced in Section 4.1, for affine transformation, the geometric and algebraic distances are identical. We use the Boat, Bark, Bikes, Graff, and Trees images from

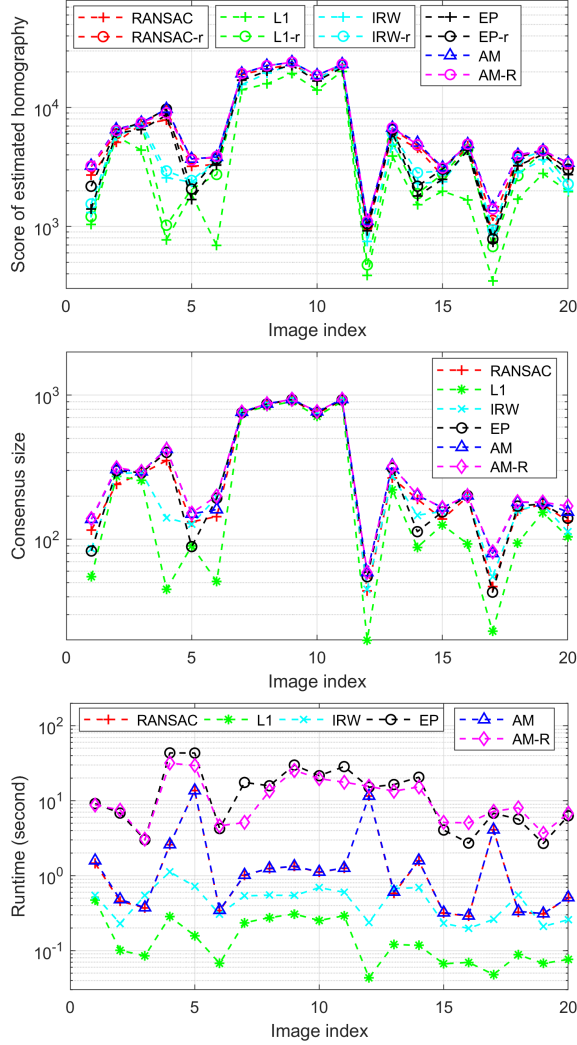


Fig. 7. Homography estimation results on 20 image pairs with geometric distance. From top to bottom are respectively the score of estimated homography, consensus size, and runtime.

the Oxford VGG’s affine image dataset. Two images pairs are picked out from each scene, which results in 10 image pairs for test. Similarly, SIFT features and correspondence matching are extracted by the VLFeat toolbox. We set an inlier threshold of $\tau = 1$ pixel for the MC algorithms, while $\beta = \Phi(\tau) = \tau^2$ for SIME. As the ground-truth transformation is unknown, we also compute a score for an estimation based on the symmetric transfer errors. For an affinity $\Theta \in \mathbb{R}^{2 \times 3}$ satisfying $\mathbf{x}_i = \Theta \tilde{\mathbf{x}}'_i$, the score is computed for $\mathbf{H} = \begin{bmatrix} \Theta \\ 0 & 0 & 1 \end{bmatrix}$ by (33).

Table 3 compares the average score of the methods, whilst Fig. 6(b) shows sample qualitative results of AM. Again, the proposed algorithms achieve the best performance in terms of average score. In the affinity estimation, the performance gap between the methods is not so prominent as that in the homography estimation experiments.

5.6 Rotation Registration

We evaluate the new algorithms on rotation search, in comparison with i) RANSAC; ii) GORE-RANSAC, which uses GORE [50] to firstly remove most outliers and then

TABLE 3
Average score of affinity estimation on 10 image pairs.

RANSAC/ RANSAC-r	L1/L1-r	IRW/IRW-r	EP/EP-r	AM	AM-R
9601/ 9688	9297/ 9498	9634/ 9697	9709/ 9715	9713	9784

uses RANSAC to estimate the model from the pruned measurements; iii) Fast global registration (FGR) [30]; iv) QUASAR [31], which is implemented in Matlab using CVX [32] with MOSEK [52] as the SDP solver. Note that GORE can provide a rough estimation of the model with guaranteed outlier removal, but GORE-RANSAC has significantly better accuracy in most cases. For QUASAR, AM and AM-R, we use the same noise bound parameter $\beta = \bar{c}^2 \sigma^2$ such that $\mathbb{P}(\|\mathbf{b}_i - \mathbf{R}\mathbf{a}_i\|^2 \leq \bar{c}^2 \sigma^2) = 1 - 10^{-6}$ holds for inliers, which under Gaussian inlier noise can be computed from the 3-DoF Chi-squared distribution. For the rotation registration problem, AM alternately solves the two subproblems (7) and (24), whilst AM-R alternately solves the two subproblems (17) and (24). We use the RANSAC solution as the initialization of AM and AM-R. All the runtime results of AM and AM-R include the runtime of the RANSAC initialization.

The Bunny dataset from the Stanford 3D Scanning Repository [53] is used. Firstly, the point cloud is resized into a unit cube $[0, 1]^3$ and randomly down-sampled to N points with $N \in \{100, 500\}$. Then, a random rotation is applied and additive noise and outliers are randomly generated according to (21). Two conditions with low and high inlier noise are considered, with $\sigma = 0.01$ and $\sigma = 0.1$, respectively. Meanwhile, different outlier ratios from 0 to 95% are considered. Each result is an average of 50 independent runs.

Fig. 8 presents the rotation error of the algorithms in the two noise conditions for $N = 100$ and $N = 500$, respectively. It can be seen that FGR performs well at low outlier ratios, but tends to beak at relatively high outlier ratios, e.g., when the outlier ratio exceeds 70% in the case of $N = 100$ and $\sigma = 0.1$. GORE-RANSAC generally has better performance than RANSAC as it firstly removes most of the outliers by the GORE method. For $N = 100$, QUASAR, AM and AM-R generally perform comparably and outperform the others. In the case of $N = 500$, QUASAR is not compared as it runs out of memory when $N > 150$. For $N = 500$, SIME distinctly outperforms its counterparts in most cases, and the advantage is especially conspicuous in the high noise case.

Fig. 9 compares the runtime of the algorithms. Clearly, FGR is the fastest. Though both QUASAR and AM-R involve solving SDP, AM-R is about 1000 times faster than QUASAR in the case of $N = 100$. This thanks to the accelerating strategy using B-M factorization and the unconstrained formulation exploiting the sparsity of the problem. However, QUASAR cannot be accelerated like AM-R as it has a large number of constraints as explained in Remark 4.

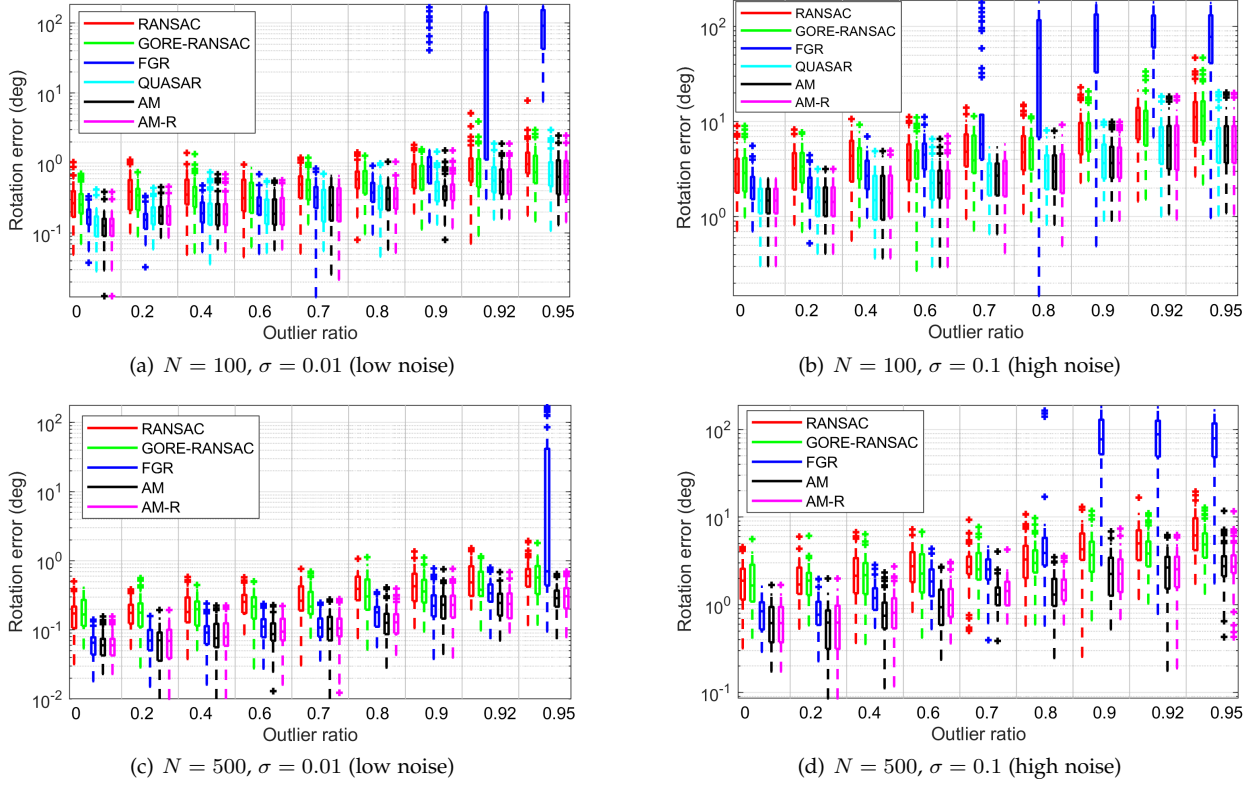


Fig. 8. Rotation error comparison in the rotation registration experiment with low and high noise conditions. (a) $N = 100, \sigma = 0.01$. (b) $N = 100, \sigma = 0.1$. (c) $N = 500, \sigma = 0.01$. (d) $N = 500, \sigma = 0.1$. QUASAR is not compared in the case of $N = 500$ as it runs out of memory when $N > 150$.

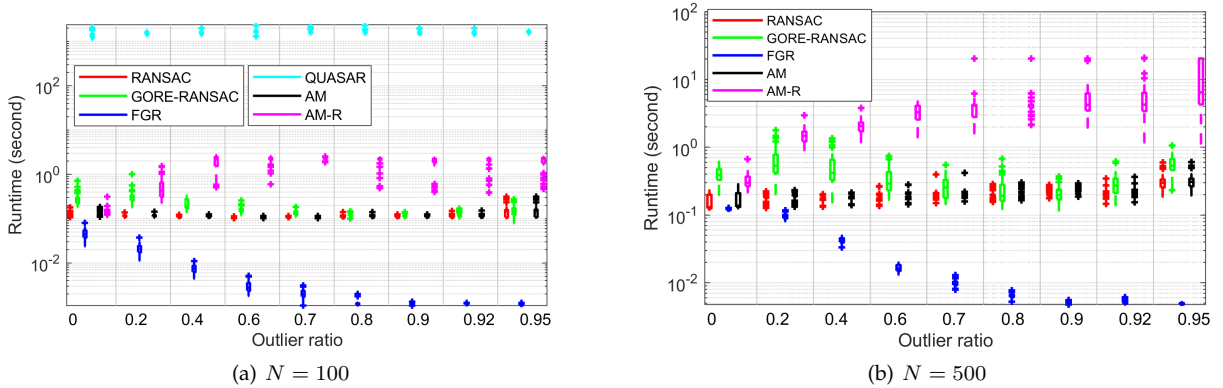


Fig. 9. Runtime comparison in the rotation registration experiment for two cases, (a) $N = 100$, and (b) $N = 500$ (with $\sigma = 0.1$).

5.7 6-DoF Euclidean Registration

The final experiment considers 6-DoF rigid registration, where both rotation and translation need to be estimated. We generate the data measurements similar to the rotation registration experiment except that a random translation is additionally considered according to (30). In this setting, AM alternately solves the two subproblems (7) and (32), whilst AM-R alternately solves the two subproblems (17) and (32). The TEASER++ algorithm (implemented in C++) [51] is also compared in this experiment. TEASER++ decouples the scale, rotation and translation estimation and solves them separately and sequentially. It solves decoupled scale and translation estimation via adaptive voting, and solves the rotation estimation via a graduated nonconvexity

scheme [29], which has shown highly effectiveness and efficiency. The noise bound parameter of TEASER++ is tuned to provide the best performance.

Fig. 10 presents the rotation error, translation error and runtime of the compared algorithms for $N = 200$. Similar to the rotation registration experiment, two noise conditions with $\sigma = 0.01$ and $\sigma = 0.1$ are considered. It can be seen that FGR tends to break at high outlier ratios, especially in the high noise condition, e.g. when the outlier ratio exceeds 50%. AM and AM-R achieve the best accuracy in most cases, and the advantage gets more prominent in the high noise condition. They again significantly outperform the RANSAC and GORE-RANSAC methods. Moreover, the results demonstrate the highly efficiency of FGR and

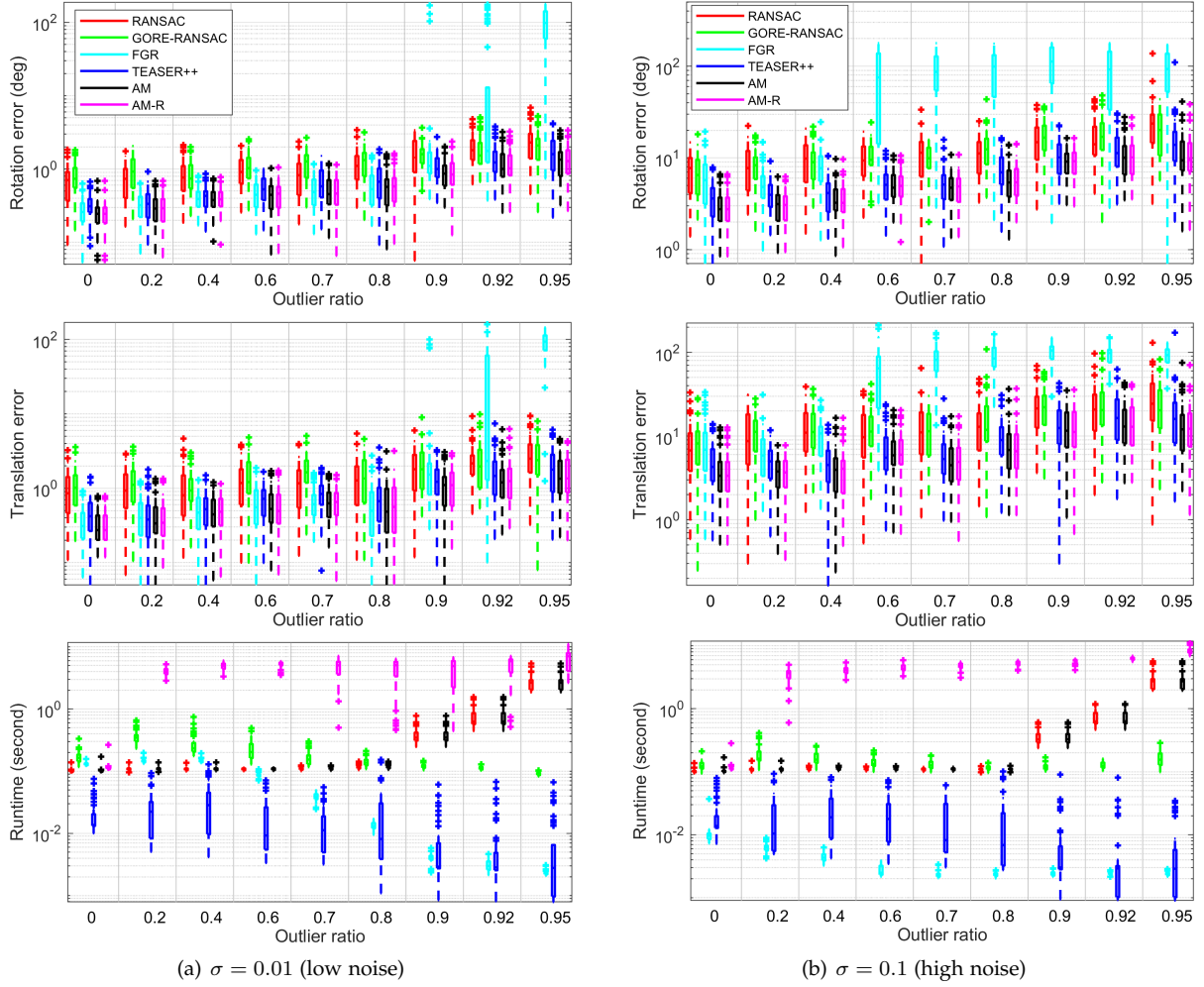


Fig. 10. Rotation error, translation error and runtime comparison in the 6-DoF Euclidean registration experiment. (a) $\sigma = 0.01$. (b) $\sigma = 0.1$.

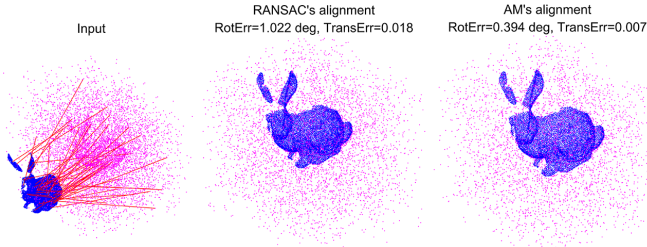


Fig. 11. Illustration of 6-DoF Euclidean registration by RANSAC and the proposed AM algorithm (with outlier ratio being 80%), along with the rotation error (RotErr) and translation error (TransErr).

TEASER++, which are much faster than AM-R. Fig. 11 illustrates a typical registration example by RANSAC and AM at an outlier ratio of 80%.

5.8 Truncated ℓ_p Loss

In the above experiments, the truncated LS loss and the truncated reprojection error have been investigated in various applications. This experiment further investigates the truncated ℓ_p loss with $1 \leq p \leq 2$. The inlier noise is generated as generalized Gaussian distribution (GGD) with

zero-mean as

$$p(x; v, \alpha) = \frac{v}{2\alpha\Gamma(1/v)} \exp\left(-\frac{|x|^v}{\alpha^v}\right), \quad (34)$$

where v is the shape parameter, α is the scale parameter, Γ is the gamma function. GGD adapts to a large family of symmetric distributions, spanning from Laplace ($v = 1$) to Gaussian ($v = 2$). When $v < 2$, the noise is super-Gaussian.

Fig. 12 shows the performance of the AM algorithm using the truncated LS and truncated ℓ_p loss in the linear regression experiment, whilst Fig. 13 shows that in the rotation registration experiment with $N = 100$. Two cases with Gaussian and GGD ($v = 0.5$) inlier noise are considered. It can be seen that in the case of GGD noise with $v = 0.5$, the truncated ℓ_p loss with a relatively small value of p (e.g. $p = 1$) can yield significant better accuracy than the truncated LS loss. A more detailed comparison in various noise conditions is provided in Appendix C.

6 Conclusion

A generalized formulation for simultaneous inlier identification and model estimation, namely SIME, has been investigated. It takes fitting residual into account in finding inliers, and is theoretically shown to have lower fitting

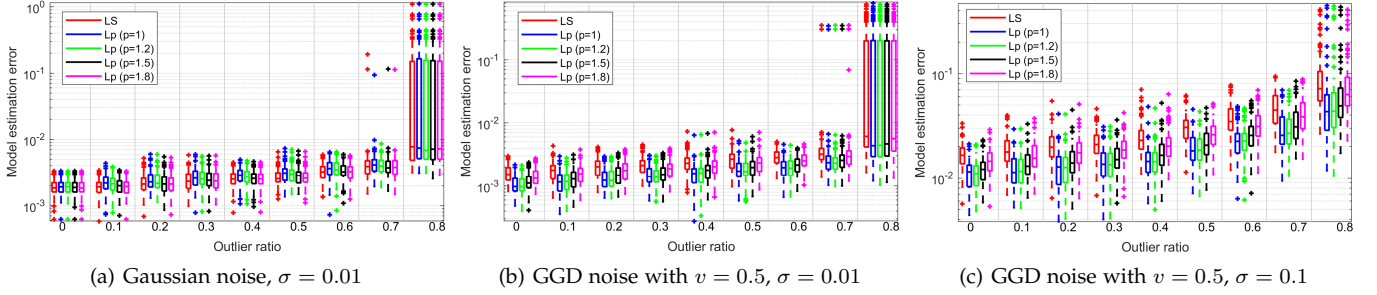


Fig. 12. Performance of the AM algorithm with truncated LS or ℓ_p loss in the linear regression experiment in the case of GGD inlier noise (with shape parameter v and standard deviation σ) and uniformly distributed outliers in $[-2, 2]$.

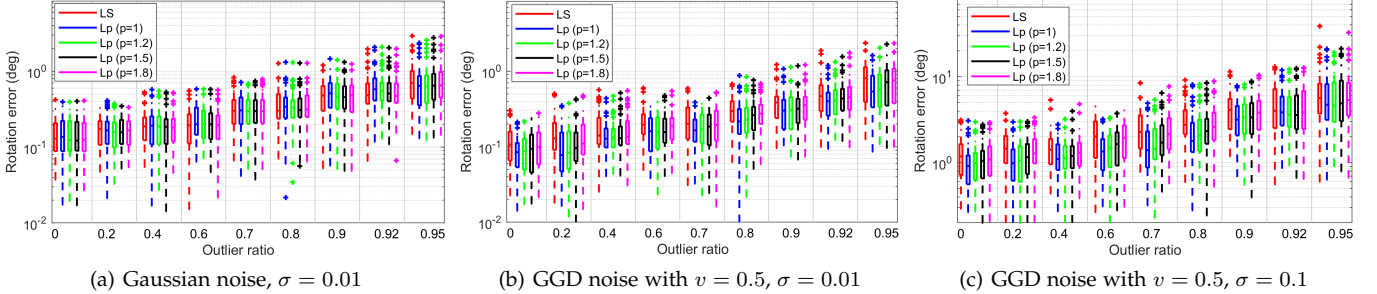


Fig. 13. Performance of the AM algorithm with truncated LS or ℓ_p loss in the rotation registration experiment (with $N = 100$) in the case of GGD inlier noise (with shape parameter v and standard deviation σ).

residual than traditional maximum consensus robust fitting. A direct AM algorithm and another one additionally using embedded SDR have been developed. The latter is further accelerated by utilizing low-rank factorization and exploiting the sparsity of the problem. Experimental results demonstrated that the new algorithms can achieve better accuracy than RANSAC and deterministic approximate maximum consensus methods at high outlier ratios. It also compares favorably with state-of-the-art registration methods in rotation and Euclidean registration, especially in the presence of high noise and outliers.

References

- [1] T. J. Chin and D. Suter, "The maximum consensus problem: recent algorithmic advances," Synthesis Lectures on Computer Vision (Eds. Gerard Medioni and Sven Dickinson), Morgan and Claypool Publishers, San Rafael, CA, USA, Feb 2017.
- [2] P. Meer, "Robust techniques for computer vision," in G. Medioni and S. B. Kang eds.: Emerging topics in computer vision. Prentice Hall, pp. 107–190, 2004.
- [3] D. Martinec and T. Pajdla, "Robust rotation and translation estimation in multiview reconstruction," in IEEE Conf. Computer Vision and Pattern Recognition (CVPR), 2007.
- [4] M. Brown and D. G. Lowe, "Automatic panoramic image stitching using invariant features," Int. J. Computer Vision, vol. 74, no. 1, pp. 59–73, 2007.
- [5] M. A. Fischler and R. C. Bolles, "Random sample consensus: a paradigm for model fitting with applications to image analysis and automated cartography," Communications of the ACM, vol. 24, no. 6, pp. 381–395, 1981.
- [6] O. Chum, J. Matas, and J. Kittler, "Locally optimized ransac," in DAGM, Springer, 2003.
- [7] B. J. Tordoff and D. W. Murray, "Guided-mlesac: Faster image transform estimation by using matching priors," IEEE Trans. Pattern Analysis and Machine Intelligence, vol. 27, no. 10, pp. 1523–1535, 2005.
- [8] O. Chum and J. Matas, "Matching with PROSAC—Progressive sample consensus," in IEEE Conf. Computer Vision and Pattern Recognition (CVPR), Jun. 2005, pp. 220–226.
- [9] S. Choi, T. Kim, and W. Yu, "Performance evaluation of RANSAC family," in British Machine Vision Conference (BMVC), 2009.
- [10] K. Lebeda, J. Matas, and O. Chum, "Fixing the locally optimized ransac full experimental evaluation," in British Machine Vision Conference, 2012, pp. 1–11.
- [11] H. Li, "Consensus set maximization with guaranteed global optimality for robust geometry estimation," in IEEE Conf. Computer Vision and Pattern Recognition (CVPR), 2009, pp. 1074–1080.
- [12] Y. Zheng, S. Sugimoto, and M. Okutomi, "Deterministically maximizing feasible subsystem for robust model fitting with unit norm constraint," in IEEE Conf. Computer Vision and Pattern Recognition (CVPR), 2011, pp. 1825–1832.
- [13] P. Speciale, D. P. Paudel, M. R. Oswald, T. Kroege, L. V. Gool, and M. Pollefeys, "Consensus maximization with linear matrix inequality constraints," in IEEE Conf. on Computer Vision and Pattern Recognition (CVPR), July 2017, pp. 5048–5056.
- [14] T. J. Chin, P. Purkait, A. Eriksson, and D. Suter, "Efficient globally optimal consensus maximisation with tree search," in IEEE Conf. Computer Vision and Pattern Recognition (CVPR), 2015, pp. 2413–2421.
- [15] O. Enqvist, E. Ask, F. Kahl, and K. Astrom, "Robust fitting for multiple view geometry," in European Conference on Computer Vision, 2012, pp. 738–751.
- [16] C. Olsson, O. Enqvist, and F. Kahl, "A polynomial-time bound for matching and registration with outliers," in IEEE Conf. Computer Vision and Pattern Recognition (CVPR), 2008, pp. 1–8.
- [17] C. Olsson, A. P. Eriksson, and R. Hartley, "Outlier removal using duality," in IEEE Conf. Computer Vision and Pattern Recognition (CVPR), pp. 1450–1457, 2010.
- [18] P. Purkait, C. Zach, and A. Eriksson, "Maximum consensus parameter estimation by reweighted L1 methods," in Int. Workshop on Energy Minimization Methods in Computer Vision and Pattern Recognition, 2018, pp. 312–32.
- [19] F. Wen, R. Ying, Z. Gong, and P. Liu, "Efficient algorithms for maximum consensus robust fitting," IEEE Trans. Robotics, vol. 36, no. 1, pp. 92–106, Feb. 2020.
- [20] H. Le, T. J. Chin, and D. Suter, "An exact penalty method for locally convergent maximum consensus," in IEEE Conf. Computer Vision and Pattern Recognition (CVPR), 2017, pp. 1888–1896.

- [21] H. Le, T. J. Chin, A. Eriksson, and D. Suter, "Deterministic approximate methods for maximum consensus robust fitting," *IEEE Trans. Pattern Analysis and Machine Intelligence*, 2019.
- [22] K. Sim and R. Hartley, "Removing outliers using the l-infinity norm," in *IEEE Conf. Computer Vision and Pattern Recognition (CVPR)*, 2006, pp. 485–494.
- [23] Y. Seo, H. Lee, and S. W. Lee, "Outlier removal by convex optimization for l-infinity approaches," in *Pacific Rim Symposium on Advances in Image and Video Technology (PSIVT)*, 2009.
- [24] S. Poljak, F. Rendl, and H. Wolkowicz, "A recipe for semidefinite relaxation for (0, 1)-quadratic programming," *Journal of Global Optimization*, vol. 7, no. 1, pp. 51–73, 1995.
- [25] S. Burer and R. D. C. Monteiro, "A nonlinear programming algorithm for solving semidefinite programs via low-rank factorization," *Mathematical Programming*, vol. 95, no. 2, pp. 329–357, 2003.
- [26] Z. Zhang, "Determining the epipolar geometry and its uncertainty: A review," *Int. J. of Computer Vision*, vol. 27, no. 2, pp. 161–195, 1998.
- [27] P. H. S. Torr and A. Zisserman, "MLESAC: A new robust estimator with application to estimating image geometry," *Comput. Vis. Image Understand.*, vol. 78, no. 1, pp. 138–156, 2000.
- [28] K. Aftab and R. Hartley, "Convergence of iteratively re-weighted least squares to robust m-estimators," in *IEEE Winter Conf. on Applications of Computer Vision*, 2015, pp. 480–487.
- [29] H. Yang, P. Antonante, V. Tzoumas, and L. Carlone, "Graduated nonconvexity for robust spatial perception: From non-minimal solvers to global outlier rejection," *IEEE Robotics and Automation Letters*, 2020.
- [30] Q. Y. Zhou, J. Park, and V. Koltun, "Fast global registration," in *European Conf. on Computer Vision (ECCV)*, pp. 766–782, 2016.
- [31] H. Yang and L. Carlone, "A quaternion-based certifiably optimal solution to the Wahba problem with outliers," in *IEEE Int. Conf. Computer Vision (ICCV)*, 2019.
- [32] M. Grant, S. Boyd, and Y. Ye. CVX: Matlab software for disciplined convex programming, 2014.
- [33] G. Pataki, "On the rank of extreme matrices in semidefinite programs and the multiplicity of optimal eigenvalues," *Mathematics of Operations Research*, vol. 23, pp. 339–358, 1998.
- [34] N. Boumal, V. Voroninski, and A. Bandeira, "The non-convex Burer-Monteiro approach works on smooth semidefinite programs," in *Advances in Neural Information Processing Systems*, 2016, pp. 2757–2765.
- [35] S. Homer and M. Peinado, "Design and performance of parallel and distributed approximation algorithm for the maxcut," *J. of Parallel and Distributed Computing*, vol. 46, pp. 48–61, 1997.
- [36] R. Fletcher. *Practical Methods of Optimization*. John Wiley and Sons, New York, second edition, 1987.
- [37] R. Hartley and A. Zisserman. *Multiple View Geometry in Computer Vision*. Cambridge university press, 2003.
- [38] Q. Ke and T. Kanade, "Quasiconvex optimization for robust geometric reconstruction," *IEEE Trans. Pattern Analysis and Machine Intelligence*, vol. 29, no. 10, pp. 1834–1847, 2007.
- [39] F. Kahl and R. Hartley, "Multiple view geometry under the ℓ_∞ -norm," *IEEE Trans. Pattern Analysis and Machine Intelligence*, vol. 30, no. 9, pp. 1603–1617, 2008.
- [40] Y. Seo and R. Hartley, "A fast method to minimize ℓ_∞ error norm for geometric vision problems," in *IEEE Conf. Computer Vision and Pattern Recognition (CVPR)*, 2007.
- [41] O. Enqvist, E. Ask, F. Kahl, and K. Åström, "Robust fitting for multiple view geometry," in *Proc. Eur. Conf. Comput. Vision*, 2012, pp. 738–751.
- [42] G. Wahba, "A least squares estimate of satellite attitude," *SIAM review*, vol. 7, no. 3, pp. 409–409, 1965.
- [43] J.-C. Bazin, Y. Seo, R. Hartley, and M. Pollefeys, "Globally optimal inlier set maximization with unknown rotation and focal length," in *European Conf. on Computer Vision (ECCV)*, pp. 803–817, 2014.
- [44] R. I. Hartley and F. Kahl, "Global optimization through rotation space search," *Int. J. of Computer Vision*, vol. 82, no. 1, pp. 64–79, 2009.
- [45] J. P. Iglesias, C. Olsson, and F. Kahl, "Global optimality for point set registration using semidefinite programming," in *IEEE Conf. on Computer Vision and Pattern Recognition (CVPR)*, 2020.
- [46] J.-C. Bazin, Y. Seo, and M. Pollefeys, "Globally optimal consensus set maximization through rotation search," in *Asian Conference on Computer Vision*, 2012, pp. 539–551.
- [47] M. D. Shuster, "A survey of attitude representations," *Journal of the Astronautical Sciences*, vol. 41, no. 4, pp. 439–517, 1993.
- [48] A. Vedaldi and B. Fulkerson, "Vlfeat: An open and portable library of computer vision algorithms," in *ACM Int. Conf. on Multimedia*, 2010, pp. 1469–1472.
- [49] R. Mur-Artal, J. M. M. Montiel, and J. D. Tardos, "Orb-slam: a versatile and accurate monocular slam system," *IEEE Trans. on Robotics*, vol. 31, no. 5, pp. 1147–1163, 2015.
- [50] A. P. Bustos and T. J. Chin, "Guaranteed outlier removal for point cloud registration with correspondences," *IEEE Trans. Pattern Analysis and Machine Intelligence*, vol. 40, no. 12, pp. 2868–2882, 2017.
- [51] H. Yang, J. Shi, and L. Carlone, "Teaser: Fast and certifiable point cloud registration," *IEEE Trans. Robotics*, 2020.
- [52] MOSEK ApS. The MOSEK optimization toolbox for MATLAB manual. Version 8.1., 2017.
- [53] B. Curless and M. Levoy, "A volumetric method for building complex models from range images," in *SIGGRAPH*, pp. 303–312, 1996.
- [54] M. Schmidt. minFunc: unconstrained differentiable multivariate optimization in Matlab. 2005.
- [55] B. K. P. Horn, "Closed-form solution of absolute orientation using unit quaternions," *J. Opt. Soc. Amer.*, vol. 4, no. 4, pp. 629–642, Apr 1987.
- [56] D. M. Rosen, L. Carlone, A. S. Bandeira, and J. J. Leonard, "SE-Sync: A certifiably correct algorithm for synchronization over the special Euclidean group," *The Int. J. of Robotics Research*, vol. 38, no. 2-3, pp. 95–125, 2019.
- [57] R. Raguram, O. Chum, M. Pollefeys, J. Matas, and J.-M. Frahm, "USAC: a universal framework for random sample consensus," *IEEE Trans. Pattern Analysis and Machine Intelligence*, vol. 35, no. 8, pp. 2022–2038, 2012.
- [58] D. Barath, J. Matas, and J. Nuskova, "Magsac: marginalizing sample consensus," in *CVPR*, 2019, pp. 10197–10205.
- [59] F. R. Hampel, E. M. Ronchetti, P. J. Rousseeuw, and W. A. Stahel. *Robust Statistics: The Approach Based on Influence Functions*. John Wiley and Sons, New York, NY, 1986.
- [60] A. Blake and A. Zisserman. *Visual Reconstruction*. The MIT Press, Cambridge, Massachusetts, 1987.
- [61] M. J. Black and A. Rangarajan, "On the unification of line processes, outlier rejection, and robust statistics with applications in early vision," *Int. J. of Computer Vision*, vol. 19, no. 1, pp. 57–91, 1996.